iScience

CellPress
OPEN ACCESS

Article

Immunopathogenic overlap between COVID-19 and tuberculosis identified from transcriptomic meta-analysis and human macrophage infection

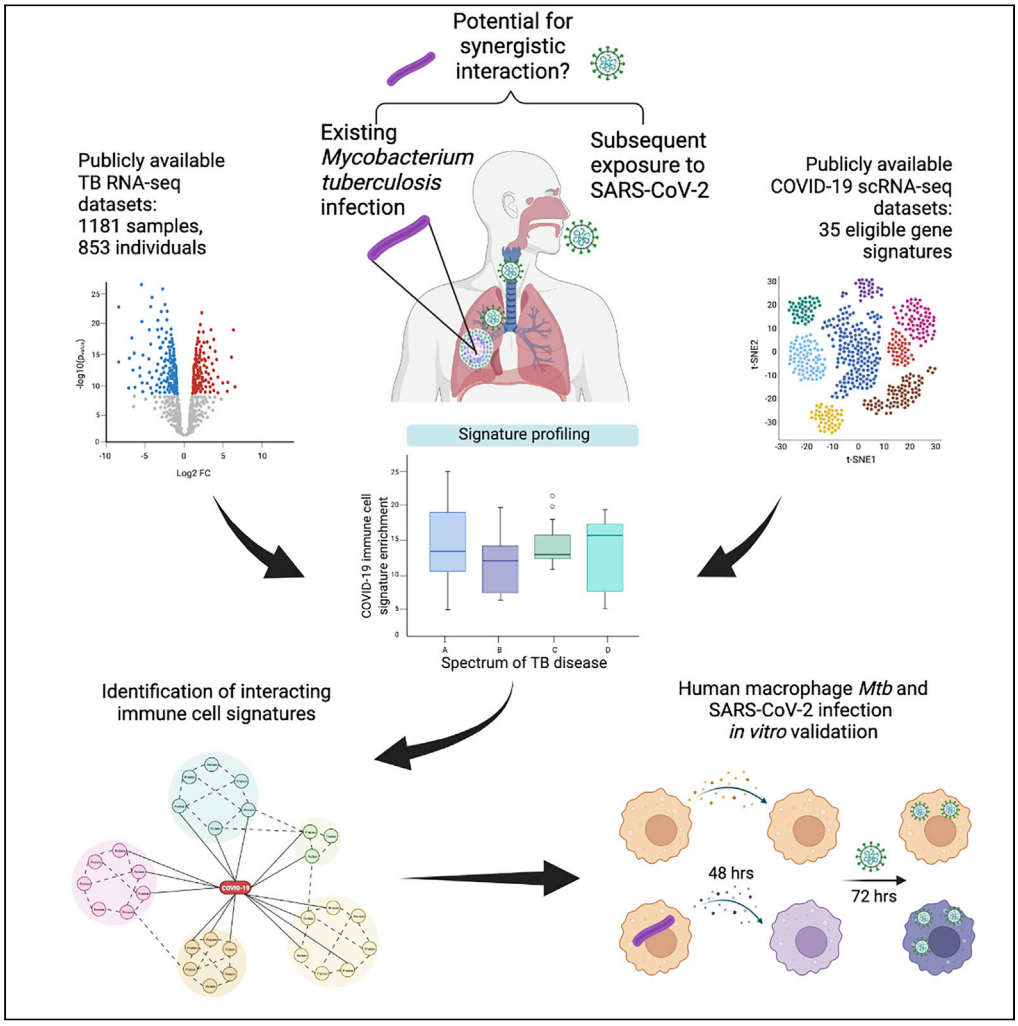

Dylan Sheerin, Abhimanyu, Nashied Peton, ..., Xutao Wang, W. Evan Johnson, Anna Kathleen Coussens

coussens.a@wehi.edu.au

Highlights

Monocyte and neutrophil COVID-19 signatures have the highest risk scores in TB

IFN-gamma and TNF signaling is enriched in COVID-19 and TB but not influenza

FCN1- and SPP1-macrophages are found in severe COVID-19 BALF and active TB blood

Mtb-induced inflammation increases human macrophage infection by SARS-CoV-2

Sheerin et al., iScience 25, 104464
June 17, 2022
https://doi.org/10.1016/j.isci.2022.104464

iScience

CellPress
OPEN ACCESS

Article

Immunopathogenic overlap between COVID-19 and tuberculosis identified from transcriptomic meta-analysis and human macrophage infection

Dylan Sheerin,[1,5] Abhimanyu,[2,5] Nashied Peton,[1,2] William Vo,[1] Cody Charles Allison,[1] Xutao Wang,[3] W. Evan Johnson,[3] and Anna Kathleen Coussens[1,2,4,6,*]

SUMMARY

Current and previous tuberculosis (TB) increase the risk of COVID-19 mortality and severe disease. To identify mechanisms of immunopathogenic interaction between COVID-19 and TB, we performed a systematic review and patient-level meta-analysis of COVID-19 transcriptomic signatures, spanning disease severity, from whole blood, PBMCs, and BALF. 35 eligible signatures were profiled on 1181 RNA-seq samples from 853 individuals across the spectrum of TB infection. Thirteen COVID-19 gene-signatures had significantly higher "COVID-19 risk scores" in active TB and latent TB progressors compared with non-progressors and uninfected controls ($p<0{\cdot}005$), in three independent cohorts. Integrative single-cell-RNAseq analysis identified *FCN1*- and *SPP1*-expressing macrophages enriched in severe COVID-19 BALF and active TB blood. Gene ontology and protein-protein interaction networks identified 12-gene disease-exacerbation hot spots between COVID-19 and TB. Finally, we *in vitro* validated that SARS-CoV-2 infection is increased in human macrophages cultured in the inflammatory milieu of *Mtb*-infected macrophages, correlating with *TMPRSS2*, *IFNA1*, *IFNB1*, *IFNG*, *TNF*, and *IL1B* induction.

INTRODUCTION

Severe acute respiratory syndrome coronavirus 2 (SARS-CoV-2) caused the first novel pandemic of the 21st century, with a global case fatality rate of 2.2% by the end of 2020 (Hasan et al., 2021), and rates of severe disease now dramatically reduced by vaccines and novel therapies. By comparison, tuberculosis (TB), similarly a respiratory-acquired infection and humanity's longest continuing pandemic, causes approximately 10 million annual cases, and has a mortality of 12–20%, the upper bound including those HIV-co-infected (World Health Organization, 2021a). TB's high mortality persists despite a vaccine that reduces infant mortality and antibiotics which have reduced mortality from roughly 50% in the pre-antibiotic era, and which still exists for drug-resistant TB. In 2020, TB and COVID-19 are estimated to have each killed roughly two million people with the number of people dying from TB increasing for the first time since 2005 (World Health Organization, 2021a; World Health Organization, 2021b).

With an estimated quarter of the world's population infected with *Mycobacterium tuberculosis* (*Mtb*), TB has remained a relatively silent killer during the COVID-19 pandemic; with the socioeconomic and health systems impacts of COVID-19 lockdowns estimated to result in an additional 6.8 million TB cases and 1.4 million TB deaths between 2020 and 2025 (Stop TB Partnership, 2020b; Zumla et al., 2020). Of growing concern to the global health community is case studies and population level data indicating TB patients, and those with latent TB infection (LTBI) or previous TB are at increased risk of severe COVID-19 (Boulle et al., 2021; Liu et al., 2020; Motta et al., 2020; Tadolini et al., 2020).

COVID-19 and TB share a symptomatic presentation of productive cough, fever, and shortness of breath, and clinical parameters of raised C-reactive protein (CRP), erythrocyte sedimentation rate (ESR), D-Dimer, interleukin (IL)-6, leukopenia, and neutrophilia. The similarity in clinical parameters and aspects of underlying immunological reactions suggests co-infection will not only complicate diagnostic algorithms, it also indicates a potentially fatal convergence in immunopathogenesis. To systematically evaluate the risk

[1]Infectious Diseases and Immune Defence Division, The Walter & Eliza Hall Institute of Medical Research, Parkville 3279, VIC, Australia

[2]Wellcome Centre for Infectious Diseases Research in Africa, Institute of Infectious Disease and Molecular Medicine, Department of Pathology, University of Cape Town, Observatory, 7925 Western Cape, South Africa

[3]Division of Computational Biomedicine and Department of Biostatistics, Boston University, Boston, MA 02118, USA

[4]Department of Medical Biology, University of Melbourne, Parkville 3010, VIC, Australia

[5]These authors contributed equally

[6]Lead contact

*Correspondence: coussens.a@wehi.edu.au

https://doi.org/10.1016/j.isci.2022.104464

posed by existing or previous TB infection on COVID-19 outcomes and vice versa, the Global Tuberculosis Network (GTN) coordinated a meta-analysis of clinical outcome of 767 TB-COVID-19 patients across 34 countries. They determined a high mortality rate of 12% in coinfected individuals and warn of a "cursed duet" requiring immediate attention (The TB/COVID Global Study Group, 2021).

To develop contextually appropriate treatment and risk mitigation interventions in communities where the syndemic potential for co-infection is high, we urgently need to understand whether the increased risk of severe COVID-19 disease and mortality identified for current and previous TB is associated with an overlap in mechanism of immunopathogenesis. The primary aim of this study was to determine whether individuals with existing TB infection, defined as those with symptomatic active TB and those with asymptomatic latent infection who were found to progress to symptomatic TB over 2 years, share a whole blood transcriptional signature which distinguishes COVID-19 patients with severe compared with mild disease. The secondary aims were to identify cellular populations and the functional pathways which contributed to the overlapping signatures of immunopathogenesis, to inform potential therapeutic mitigation strategies, and validate detrimental interactions via *in vitro* infection.

The impact of dual infection is best assessed by comparing the effect of one pathogen on the immune response before and following a subsequent co-infection event. In the absence of data from longitudinal studies where samples are available from *Mtb*-infected individuals before and during SARS-CoV-2 infection, we first wanted to test whether transcriptional signatures of increased risk of severe COVID-19 exist in *Mtb*-infected individuals, before co-infection, which will inform data acquired from future prospective longitudinal cohorts of acquired co-infection. We therefore conducted a systematic review of whole blood (WB), peripheral blood mononuclear cell (PBMC) and bronchoalveolar lavage fluid (BALF) signatures associated with COVID-19 clinical severity and performed a meta-analysis against WB RNA-seq data from individuals across the spectrum of asymptomatic and symptomatic TB infection. This was complemented with an integrative single-cell (sc)RNA-seq comparison between COVID-19 and TB patients and gene set enrichment analysis (GSEA) to identify cellular and systems level convergence of immunopathogenesis. Our findings suggest that subclinical and active TB (ATB) may increase the risk of severe COVID-19 disease because of increased abundance of circulating myeloid subpopulations also found in the lungs of severe COVID-19 patients. Shared myeloid and platelet-associated oxidative stress pathways of immunopathogenesis suggests that SARS-CoV-2 co-infection could also trigger progression of subclinical to active TB and we identify 12 gene exacerbation hotspots as potential therapeutic targets for treating co-infection. Finally, we demonstrate that *Mtb* infection induces *ACE2* and *TMPRSS2* expression in human macrophages, that SARS-CoV-2 infection is increased in human macrophages co-incubated in the inflammatory milieu from *Mtb*-infected macrophages, and this correlates with induced expression of *TMPRSS2*, *IFNA1*, *IFNB1*, *IFNG*, *IL1B*, and *TNF*.

RESULTS

COVID-19 signature meta-analysis in TB

The hypothesis that WB transcriptomic signatures present in those with existing *Mtb* infection will increase risk of severe COVID-19 and that immunopathogenic overlap during co-infection will increase the likelihood of asymptomatic latent/subclinical TB progressing to active disease was evaluated using a combination of transcriptomic data from COVID-19 patients and WB RNA-seq data from studies of TB disease progression on which the COVID-19 signatures were evaluated. Following systematic review of the published and preprint manuscripts, nine COVID-19 studies met inclusion criteria (Table 1, Figures S1 and S2) (Arunachalam et al., 2020; Hadjadj et al., 2020; Huang et al., 2020; Liao et al., 2020; Silvin et al., 2020; Wei et al., 2020; Wen et al., 2020; Wilk et al., 2020; Xiong et al., 2020) and were used to generate 35 tissue-level, cell-level, or pathway-level signatures of varied severity risk for evaluation (Table S1). A WB influenza microarray dataset (Table 1)(Dunning et al., 2018) was used to generate a respiratory viral control signature by contrasting healthy controls with H1N1 patients. Funnel plot analysis was used to assess any publication bias in selected studies (Figures S3).

The curatedTBData package (Wang, 2020), which includes 48 publicly available TB RNA-seq datasets, was used to identify eligible WB TB datasets, that included individuals who progressed to TB during the duration of study follow-up, with RNA-seq data at baseline and time of diagnosis, and patient-level meta-data including time to TB progression. Three prospective TB cohort studies encompassing 853 individuals and 1181 samples, at various time points, were eligible for comparison (Figure S2 and Table 2) (Singhania et al., 2018; Suliman et al., 2018; Zak et al., 2016).

Table 1. Characteristics of COVID-19 studies used to derive signatures for COVID-19 risk profiling on tuberculosis datasets

Study	Tissue	Sequencing platform	Cohort	Severity	Eligible signatures	Signature type
Wilk et al., (2020)	PBMCs	Seq-Well	7 patients hospitalized with confirmed COVID-19 (all male, aged 20-80 + yrs.), 6 healthy controls	3 COVID-19 patients were on ventilation and diagnosed with ARDS; 4 were less severely ill patients. Samples collected 2-16 days following symptom onset	4	Monocytes, NK cells, "activated granulocytes", and interferon sensitivity genes
Huang et al., (2020)	PBMCs	10X Chromium	8 active disease patients, 2 cured patients, 3 healthy controls, and non-COVID-19 patients	Active disease patients: 1 critical case, 1 severe case, 6 moderate cases. Non-COVID-19 patients: 1 case of influenza A, 1 case of acute pharyngitis, and 1 case of cerebral infarction	1	Interferon
Wen et al., (2020)	PBMCs	10X Chromium	10 recovering patients (5 male, 5 female, aged 40-70 years), plus healthy controls	5 early-recovery stage (ERS) and 5 late-recovery stage (LRS) patients, classified by days between blood sampling date and negative qPCR	5	Monocytes, NK cells, CD4 T cells, CD8 T cells, B cells
Liao et al., (2020)	BALF	10X Chromium	6 COVID-19 patients (5 male, 1 female, median age: 49.5), 8 previously reported healthy lung controls	3 severe, 3 mild	6	Macrophages (G1–G4), CD8 T cells
Xiong et al., (2020)	BALF and PBMCs	MGISEQ-2000	3 COVID-19 patients and 3 healthy controls	No severity information provided	2	PBMC and cytokine
Hadjadj et al., (2020)	Whole blood	nanoString nCounter	50 COVID-19 patients with a spectrum of disease severity	15 mild/moderate, 17 severe, and 18 critical	5	Interferon sensitivity genes, whole blood, mild/moderate, severe, critical
Wei et al., (2020)	PBMCs	10X Chromium	4 COVID-19 patients	Patients sampled before, during, and after ICU care	4	Inactivated monocytes, classical monocytes, T cells, B cells
Silvin et al., (2020)	Whole blood	10X Chromium	3 COVID-19 patients and 3 healthy controls	1 mild, 2 severe patients sampled at day 0 and day 10	3	Monocytes, neutrophils, whole blood
Arunachalam et al., (2020)	PBMCs	10X Chromium	7 COVID-19 patients and 5 healthy controls	No severity information provided for scRNA-seq samples	5	PBMC, moderate, severe, intensive care unit, blood transcriptional module
Dunning et al., (2018)	Whole blood	Illumina GenomeStudio	131 influenza patients, 155 healthy controls	Not applicable	1	Whole blood

ARDS, acute respiratory distress syndrome. BALF, bronchoalveolar lavage fluid; ICU, intensive care unit. NK, natural killer. PBMC, peripheral blood mononuclear cells. scRNA-seq, single cell RNA sequencing. See also Figures S1, S2, and S3 and Table S1.

COVID-19 signatures were first evaluated in the TB combined observational and prospective cohort (TCC), including 293 individuals from the UK (London and Leicester) and South Africa, and 414 time-point samples (Singhania et al., 2018). Out of the 35 COVID-19 signatures profiled, 20 were significantly associated ($p<0{\cdot}005$) with higher COVID-19 risk scores in TB patients and recent TB contacts who progressed to TB over 1-2 years (i.e., with subclinical TB), compared with UK latently infected individuals (Table S2). By comparison to another respiratory infection, the pneumonic influenza signature score centered on zero across the TB spectrum (Figure 1).

The mild/moderate and severe COVID-19 WB signatures (Hadjadj et al., 2020) (Figure 1) showed significant differences in COVID-19 risk scores between ATB and LTBI ($p<0{\cdot}00001$ and $p<0{\cdot}005$, respectively) while the critical COVID-19 signature generated a comparatively lower risk score in the TB groups, but was

Table 2. Characteristics of the TB datasets used to profile COVID-19 risk from COVID-19 immune cell and pathway signatures

Dataset	Setting	Samples included	Study design	Population	Sampling	TB case definition	Follow-up duration and method
TB contacts cohort (TCC) (Singhania et al., 2018)	London, UK	54 (21 active TB, 33 LTBI non-progressors)	Cohort	HIV-negative adults (18–78 years) TB cases and TB contacts	Baseline	TB: Culture confirmed or clinically diagnosed LTBI: QFT positive	1.9 years (IQR, 1.7–2.2)
	Cape Town, South Africa	47 (16 active TB, 31 LTB non-progressors I)					
	Leicester, UK	313 (53 active TB, 23 progressors, 118 LTBI non-progressors, 119 healthy non-progressors)	Cohort	HIV-negative individuals (16–84 years) TB cases and TB contacts	Baseline plus serial for a sub-set	TB: Culture-confirmed or GeneXpert MTB/RIF positive LTBI: QFT positive	13 months, active
Adolescent cohort study (ACS) (Zak et al., 2016)	Cape Town, South Africa	355 (110 progressors, 245 matched non-progressors)	Nested case-control	HIV-negative adolescents (12–18 years) with latent TB infection	Serial (0, 6, 12, and 24 months)	TB: Intrathoracic disease with 2 positive smears or 1 positive culture LTBI: QFT positive	2 years, active
Grand Challenges 6 (GC6) (Suliman et al., 2018)	The Gambia South Africa Ethiopia	412 (98 progressors, 314 matched non-progressors)	Nested case-control	HIV-negative individuals (8–60 years) household pulmonary TB contacts	Serial (0, 6, and 18 months)	TB: Culture confirmed or clinically diagnosed LTBI: QFT positive	2 years, active

LTBI, latent TB infection; QFT, QuantiFERON-TB. See also Figure S2.

significantly higher in the Leicester ATB cases vs LTBI ($p<0{\cdot}0001$). COVID-19 disease severity blood transcriptional module (BTM) signatures (Silvin et al., 2020) included genes involved in interferon (IFN) responses and antigen processing and presentation and clearly separated ATB patients from all others ($P<0{\cdot}0001$).

Of the 20 scRNA-seq immune cell population signatures profiled, innate immune cell signatures generated the highest COVID-19 risk scores in active and progressive TB. The classical monocyte signature (Wei et al., 2020) found to be drastically increased in ICU cases of COVID-19, yielded the most significantly increased risk scores between latent and active TB ($p<0{\cdot}0001$). The COVID-19 WB neutrophil signature (Silvin et al., 2020) was most significantly increased in active vs latent TB ($p<0{\cdot}0001$). The lung macrophage subpopulations associated with severe disease in bronchoalveolar lavage fluid (BALF) from COVID-19 patients (Liao et al., 2020) also showed high risk scores; in particular, the $FCN1^{hi}$ (monocyte-derived macrophages (MDM), G1), $FCN^{lo}SPP1^{hi}$ (pre-fibrotic macrophages, G2), and intermediary G1/2 macrophages.

Conversely, the majority of adaptive immune cell signatures ($CD4^+$ and $CD8^+$ T cells) were higher in LTBI and TB contacts who did not progress to TB (Figure 1). Of the ten COVID-19 signatures that were not associated with a significantly higher COVID-19 risk score in ATB, seven originated from T cells and B cells and were enriched in mild vs. severe COVID-19 in the original studies. In general, T cell populations are depleted during severe COVID-19 infection (Liao et al., 2020; Wei et al., 2020; Wen et al., 2020) and a lower COVID-19 risk score for these signatures in the active and progressive TB patients could reflect a similar peripheral depletion of these populations in TB. In patients recovering from COVID-19 (Wei et al., 2020), their monocyte signature was associated with the early recovery stage during persistence of hyperinflammation, whereas the NK cell, T cell, and B cell signatures were enriched in the late recovery stage, likely explaining the low COVID-19 risk scores associated with these later signatures in ATB.

Assessing COVID-19 risk scores after further stratifying the Leicester TB contacts and ATB index cases by the phenotype of index case TB (pulmonary [PTB] or extrapulmonary [EPTB]) revealed higher COVID-19 risk

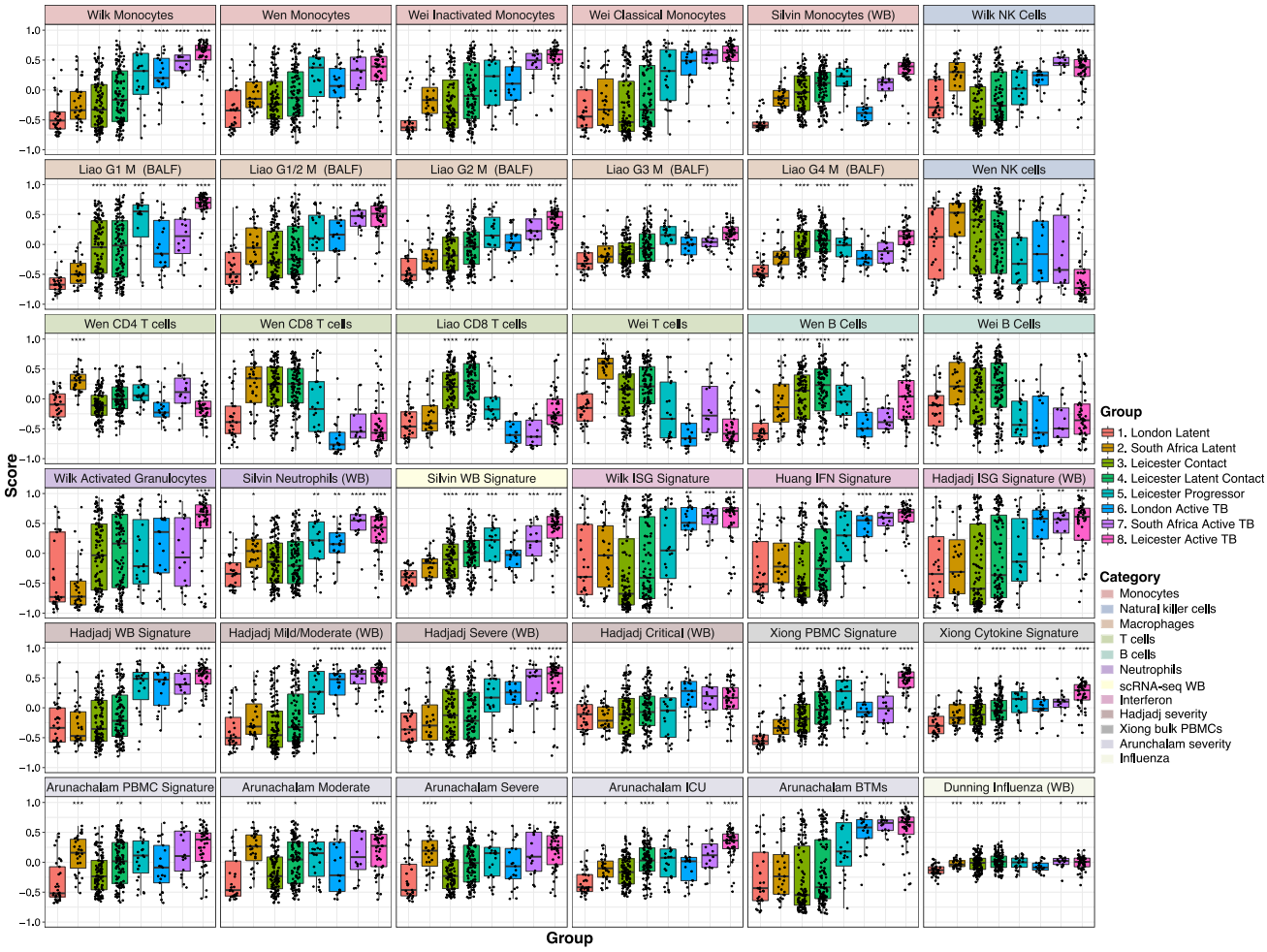

Figure 1. Profiling immune cell signatures from COVID-19 patients highlights increasing risk of severe disease associated with progression to active tuberculosis

COVID-19 immune cell signatures were derived from bulk and single-cell RNA-sequencing (RNA-seq) studies and used to generate putative "COVID-19 risk scores" from a tuberculosis (TB) whole blood bulk RNA-seq dataset using the TBSignatureProfiler package. TB samples are grouped according to disease state and COVID-19 signatures were categorized by immune cell or signature type. Scores for each signature were compared by contrasting each group with the 'London Latent' group using a *t*-test with Bonferroni correction. All signatures were derived from peripheral blood mononuclear cells (PBMCs) unless otherwise stated in the boxplot title. Each individual signature title is prefixed by the first author of the study from which it was derived. Category colors relate to cell type, disease, pathway or study first author. WB, whole blood. M, macrophage. BALF, bronchoalveolar lavage fluid. ISG, interferon (IFN)-stimulated gene. NK, natural killer. ICU, intensive care unit. BTM, blood transcriptional module. Boxplots denote median and 25th to 75th percentiles (boxes) and 10th to 90th percentiles (whiskers). *, p<0·05; **, p<0·005; ***, p<0·0005; ****, p<0·00005. See also Tables 1, 2, S1, and S2.

scores in PTB vs EPTB patients and that TB progressors who were contacts of PTB, had higher COVID-19 BALF and WB signature scores closer to time of TB diagnosis (Figure 2 and Table S3).

Thirteen signatures having significantly higher COVID-19 risk score (adjusted p<0·005) in at least two ATB groups, compared with LTBI, were selected for validation in two additional prospective TB progressor RNA-seq datasets: the ACS (Zak et al., 2016) and GC6 (Suliman et al., 2018) cohorts, including 153 and 407 individuals, respectively (Table S4). Both datasets exhibited the same trend of increased COVID-19 risk score for all 13 signatures in individuals with LTBI who progressed to TB vs. those who did not ($p \leq 0{\cdot}01$), whilst scoring a zero median for the influenza signature (Figure 3 and Table S4). The COVID-19 IFN signatures (Hadjadj et al., 2020; Huang et al., 2020; Wilk et al., 2020) were associated with the greatest difference in COVID-19 risk score between LTBI and TB progressors (p<0·001) in both cohorts. Plotting by days to TB diagnosis revealed an additional trend of higher risk score associated with proximity to ATB disease in the ACS cohort (Figure 3A) but not the GC6 cohort (Figure 3B).

Figure 2. Profiling immune cell signatures from COVID-19 patients highlights increasing risk of severe disease among contacts of pulmonary tuberculosis patients

Scores for each signature were compared by contrasting each group with the contact (extrapulmonary) group using a *t*-test adjusted for multiple testing using a Bonferroni correction. WB, whole blood. M, macrophage; BALF, bronchoalveolar lavage fluid. ISG, interferon (IFN)-stimulated gene. NK, natural killer. ICU, intensive care unit. BTM, blood transcriptional module. Boxplots denote median and 25th to 75th percentiles (boxes) and 10th to 90th percentiles (whiskers). *, p<0·05; **, p<0·005; ***, p<0·0005; ****, p<0·00005. See also Tables 1, 2, S1, and S3.

COVID-19 lung and TB blood enriched in inflammatory monocyte sub-lineages

Reported similarities between BALF and WB scRNA-seq expression profiles observed in COVID-19 patients led us to investigate whether the BALF macrophage sub-lineages (Liao et al., 2020) that associated with COVID-19 risk in ATB patients (Figure 1) could be detected in circulation during TB infection. An integrated scRNA-seq analysis was performed using publicly available TB scRNA-seq PBMC data (Cai et al., 2020), consisting of both active and LTBI samples, with BALF scRNA-seq data from COVID-19 patients of varying disease severity (Figure S4) (Liao et al., 2020). A high concordance was observed between the immune cell populations present within ATB PBMC and severe COVID-19 BALF after t-distributed stochastic neighbor embedding (tSNE) dimensionality reduction (Figure 4A). Canonical cell type marker genes were identified for each cluster and assigned to the tSNE plot to identify shared and unique subpopulations (Figure 4B). Three major macrophage sub-lineage markers identified in the original BALF scRNA-seq analysis, *FCN1*, *SPP1*, and *FABP4*, were separately profiled on the macrophage clusters of the COVID-19 and TB samples (Figure 4C). The *FCN1*-expressing pro-inflammatory monocyte-derived macrophage population was the most abundant of the sub-lineages in severe COVID-19 patients (Liao et al., 2020), and had highest expression in the TB PBMC, whereas *FABP4*, an alveolar macrophage subset marker, was completely absent in TB PBMC. Zooming in on the *FCN1*-expressing and *SPP1*-expressing clusters,

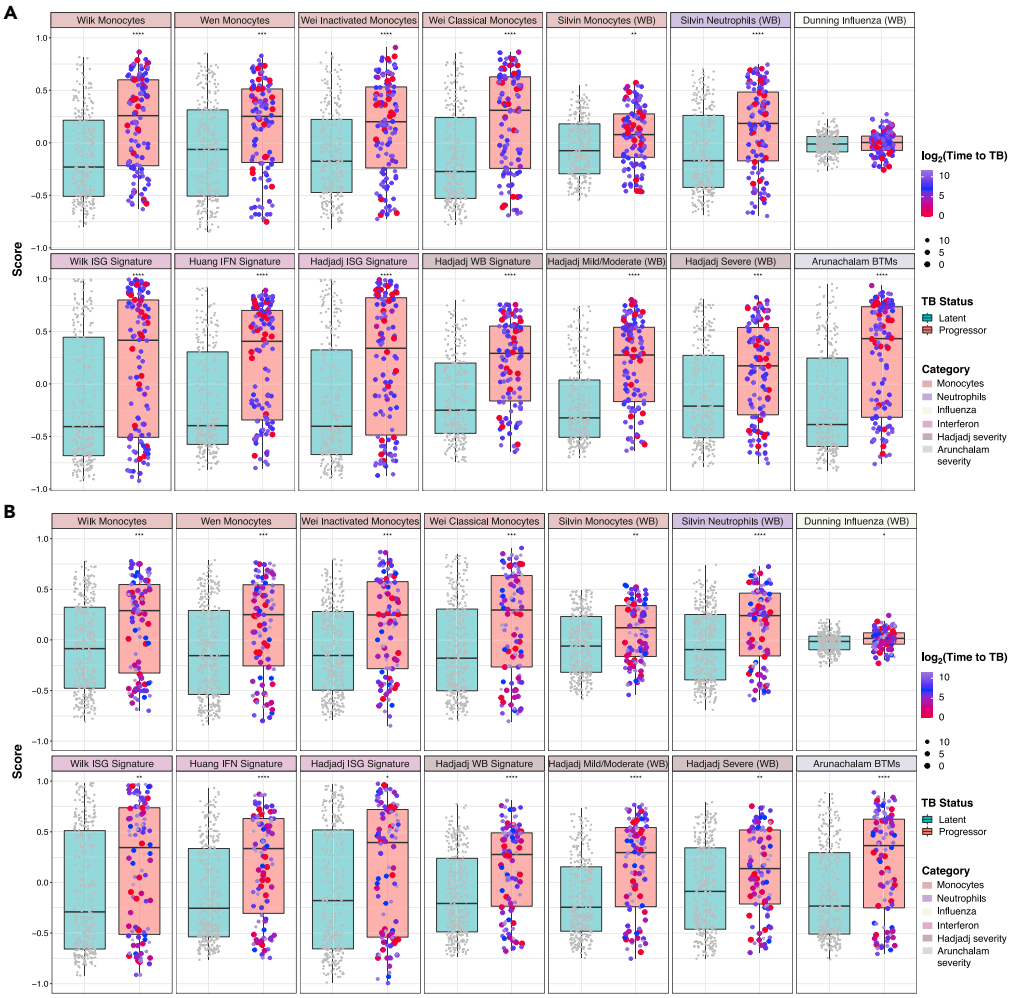

Figure 3. Risk of developing severe COVID-19 is significantly elevated in patients that progress from latent to active tuberculosis disease

COVID-19 immune cell signatures that were associated with significant differences in COVID-19 risk score between controls and progressor/active tuberculosis (TB) cases were validated on two additional whole blood (WB) RNA-sequencing TB datasets - (A) the Adolescent Cohort Study (ACS) and (B) the Grand Challenges 6 (GC6) study. TB samples were classified as latent or progressors and COVID-19 signatures were categorized by immune cell or signature type. Samples from patients that progressed to active TB disease during the study follow-up period are colored and scaled according to time to TB diagnosis, measured in days and plotted on a $\log_2$ scale. Scores for each signature were compared by contrasting progressors with latent cases using a *t*-test with Bonferroni correction. All signatures were derived from whole blood unless otherwise stated in the boxplot title. Boxplots denote median and 25th to 75th percentiles (boxes) and 10th to 90th percentiles (whiskers). *, p<0·05; **, p<0·005; ***, p<0·0005; ****, p<0·00005. See also Tables 1, 2, S1, and S4.

the additional inflammatory markers that were identified for these populations in the original analysis (*CD68*, *S100A8*, *CCL2*, *CCL3*, *CD14*, and *CXCL10*) were profiled. Both ATB and severe COVID-19 samples had high expression of these markers (Figure 4D) indicating that pro-inflammatory monocyte sub-lineages enriched in the lung of severe COVID-19 are abundant in the circulation of ATB patients.

Convergence of enriched pathways in COVID-19 and TB

To gain a greater understanding of synergistic pathogenic mechanisms to inform therapeutic targets for treating co-infection, a meta-pathway enrichment analysis was performed, using the transcriptomic data from the Leicester TB (Singhania et al., 2018), the COVID-19 WB scRNA-seq data (Silvin et al., 2020), and the influenza viral control cohort (Dunning et al., 2018). Among the top 1000 differentially expressed genes

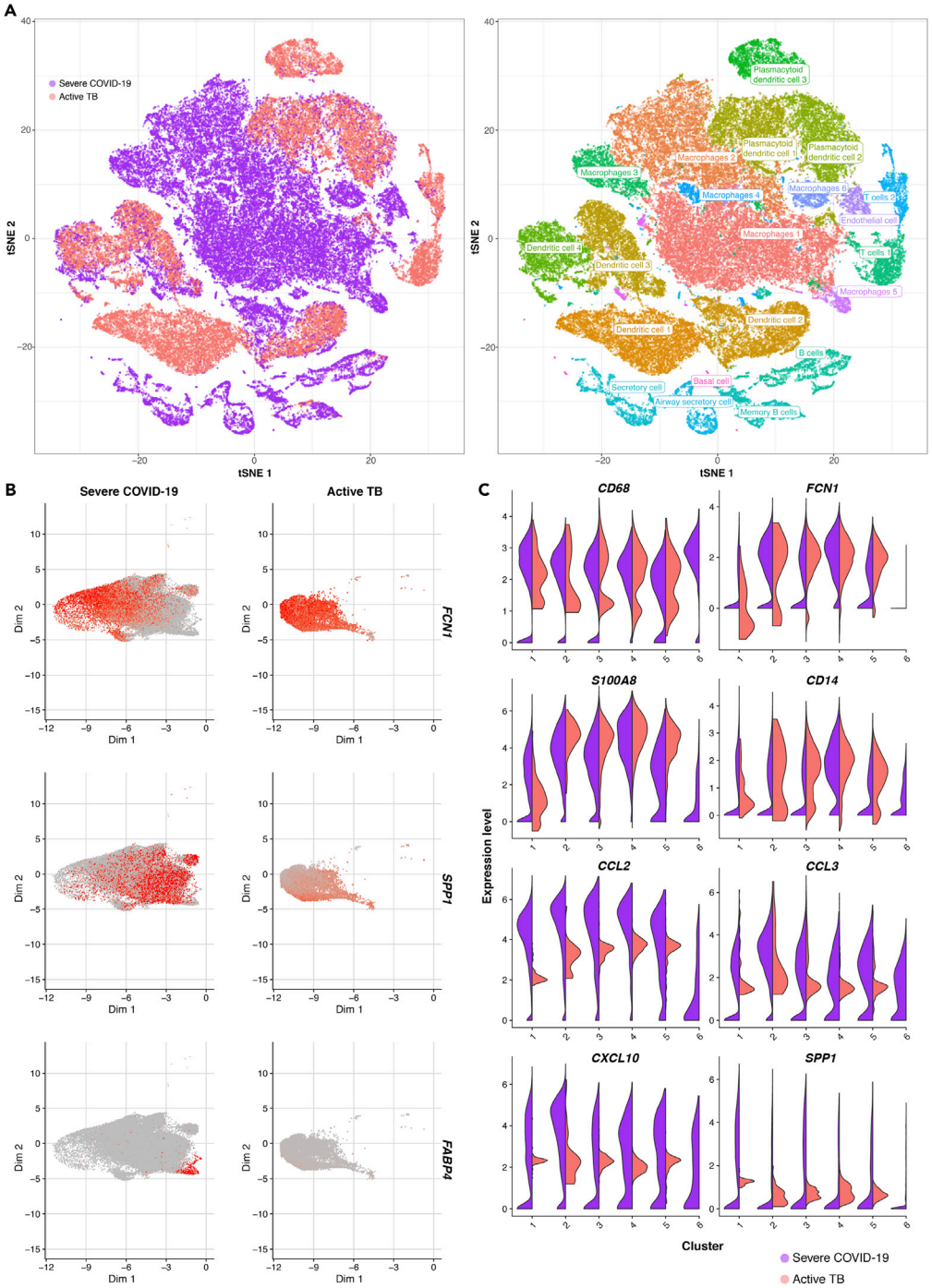

Figure 4. Macrophage subpopulations upregulated in the lungs of severe COVID-19 patients can also be found in the circulation during active tuberculosis disease

Single-cell RNA-sequencing (scRNA-seq) data from bronchoalveolar lavage fluid (BALF) of severe COVID-19 patients (n = 6) and peripheral blood mononuclear cells (PBMCs) from patients with active tuberculosis (TB) disease (n = 3) were integrated.

(A) t-distributed stochastic neighbor embedding (tSNE) plot of integrated scRNA-seq data in the left panel, with cells from severe COVID-19 patients in guava and those from active TB patients in cyan, with corresponding cell clusters annotated based on identified markers in the right panel.

Figure 4. *Continued*

(B) Macrophage clusters from the severe COVID-19 patients (left column) and active TB patients (right column), with the expression of major macrophage subpopulation markers identified in the original COVID-19 study - *FCN1*, high in G1, low in G2; *SPP1*, G2, and G3; *FABP4*, G4 - highlighted in red.

(C) Violin plots depicting the expression levels of additional inflammatory marker genes associated with the macrophage subpopulations also present in the TB PBMC data, for each macrophage cluster. Violin plots denote frequency distribution curves of the 25th to 75th percentiles (shaded) and 10th to 90th percentiles (whiskers). See also Figure S4.

(DEGs) across all datasets, COVID-19, ATB, and TB progressors shared the greatest overlap, compared with LTBI or influenza (Figure S5). Comparing the 20 most significant ontologies (Figure 5A and Table S5), COVID-19 could be distinguished from influenza on the basis of the presence of IFN-γ and TNF response pathways; however, these were both highly enriched in ATB and TB progressors and to a lesser extent in LTBI. Conversely, LTBI had no enrichment of cytokine production and regulation of innate immune response, compared with the other disease states. Among the top 100 pathways there were four major clusters of pathways: 14 pathways shared across all disease states, 39 shared by COVID-19, ATB, TB progressors and influenza, but not LTBI, 20 shared exclusively with COVID-19, ATB and TB progressors, and a further nine also shared with LTBI, but not influenza (Figure 5B and Table S6).

To identify key effector genes responsible for the activation of enriched pathways, significant protein-protein interaction (PPI) network clusters were generated (Figure 5C) using a meta-pathway analysis approach, identifying enriched Molecular Complex Detection (MCODE) complexes which were then annotated by gene ontology (GO) (Figure S6 and Table S7). Among the 85 DEGs which were represented in the eleven identified MCODE networks (Table S8), only nine genes were differentially expressed in influenza of which only three were shared with COVID-19. Conversely, 33 genes were shared in PPI networks between COVID-19 and at least one TB state, with 12 of these genes (*BCL6*, *CD74*, *JNB*, *LCP1*, *HLA-A*, *HLA-DPA1*, *NCF1*, *PSME2*, *SLC2A3*, *SPI1*, *STAT3*, and *TLN1*) enriched in COVID-19, ATB, and TB progressors (Figures 5C and S7). Antigen processing and presentation (dominated by HLA genes) and epigenetic regulation (dominated by genes encoding histone-related proteins, and epigenetic regulators [e.g., *EP300*, *CREBBP*, and *SLC2A3*]) were the largest two MCODE networks shared between COVID-19 and active and progressive TB. Other co-enriched networks in COVID-19 and TB included genes involved in reactive oxygen and nitrogen species production (e.g., *NCF1, NCF2, and CYBA*), platelet activation (e.g., *TLN1, RAC2*), cytokine production (e.g., *STAT1*, *STAT3, and IL15RA*), and transcriptional regulation (e.g., *SPI1*, *BCL6*, and *JUNB*).

Among the top 100 enriched pathways only one pathway, Hallmark of mTORC signaling, was unique to COVID-19 and absent across the spectrum of TB and influenza (Figure 6A). To explore which of the top 100 enriched pathway DEGs were associated with severity of COVID-19, and assess enrichment in other diseases, GSEA was used to determine enrichment of three distinct pathway clusters identified, excluding a fourth pathway cluster that was shared between all diseases (Figure 6A), in a WB bulk RNA-seq dataset containing samples from moderate, severe and ICU COVID-19 patients (Figures 6B and S8) (Arunachalam et al., 2020). Pathway cluster one comprising IFN-γ response, apoptotic signaling, and B cell activation, common to COVID-19 and all TB states but absent from influenza, was found to be enriched in all three COVID-19 disease severity categories with moderate effect size. Conversely, pathway clusters two and three had larger effect sizes in the more severe COVID-19 disease states (Table S9). Cluster two comprising complement activation, inflammatory response, apoptotic signaling, T cell receptor signaling, and IFN-γ production, was common across all disease groups, except LTBI. Cluster three comprising platelet degranulation, autophagy, antigen processing and presentation, TNF signaling, IL-6/JAK/STAT3 signaling, and metabolic response to infection, was shared between COVID-19, ATB, and TB progressors but absent from LTBI and influenza. Signature profiling was performed on the three cluster-specific DEGs in the UK and SA TB cohorts. For the three cluster-specific DEGs, groups ranging from TB progressors to ATB showed significant COVID-19 risk scores compared with the LTBI groups, with cluster three, which contains the most shared DEGs between COVID-19, ATB, and TB progressors, exhibiting the strongest graded increase in COVID-19 risk scores (Figure 6C and Table S10).

Inflammatory milieu from *Mtb*-infected human macrophages increases SARS-CoV-2 infection *in vitro*

To validate a detrimental inflammatory interaction between existing *Mtb* infection and subsequent SARS-CoV-2 infection, the likely sequence of co-infection given a quarter of the world is estimated to have been infected with *Mtb* (Houben and Dodd, 2016), we assessed the impact of an *Mtb*-induced

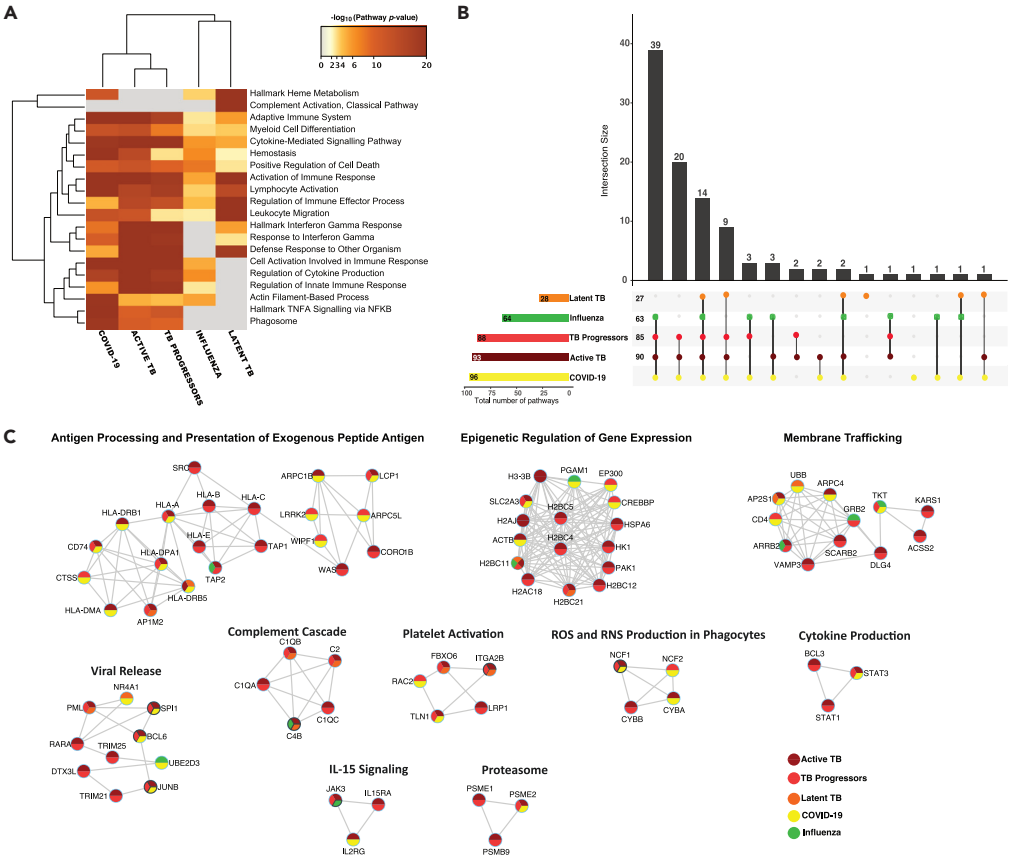

Figure 5. Active TB disease and COVID-19 have similar perturbed pathways and gene networks

(A) Heatmap of the top 20 most significant enriched pathways ($p<0.001$) from the meta-analysis across the five groups. Cells are colored by their $-\log_{10}$(p-values), gray cells indicate no significant enrichment for that term/ontology in the corresponding differentially expressed genes (DEGs) list (see Table S5).

(B) Upset intersection plot showing the number of pathways shared between COVID-19 and the other groups. Wherever the genes are shared the specific-coloured dots appear below the column bar graph which shows the number of shared pathways, which are connected by vertical lines, denoting shared categories. The horizontal bars represent the category gene count and the numbers on the horizontal axes represent the common pathways between the represented category and COVID-19 (see Table S6).

(C) All MCODE components from a protein-protein interaction (PPI) network analysis of the top 1000 DEG from all merged gene lists are displayed for the top 10 networks, nodes are displayed as pie charts, color coded by disease group. Cluster labels are derived from functional labels based on the top three enriched terms for that MCODE cluster (see Figure S6 and Table S7). Cluster membership is derived from the available gene expression data from the top 1000 DEG in the analysis (see Table S8 and Figure S7).

inflammatory microenvironment on human MDM susceptibility to SARS-CoV-2 infection (Figure 7). Seven-day GM-CSF-derived pro-inflammatory MDM were chosen for *in vitro* infection, given our finding of *FCN1*^{hi} pro-inflammatory MDM as the most abundant immune population shared between severe COVID-19 BALF and PBMC of TB patients in scRNA-seq analysis (Figure 4). MDM were first infected with an *Mtb* clinical isolate (MOI 1) for 4 hrs, followed by removal of extracellular *Mtb* by washing, and cultured up to 48 hrs. Gene expression of key inflammatory cytokines, *ACE2* (SARS-CoV-2 receptor) and *TMPRSS2* (key protease required for spike cleavage and ACE2 engagement) assessed at 24, 36 and 48 hrs to determine the impact of *Mtb* infection on MDM susceptibility to SARS-CoV-2 infection and associated inflammatory milieu.

TNF and *IL1B* were significantly increased at all three time points. *IFNG* had the largest induction of expression at 24 hrs, which decreased over 36–48 hrs, whereas *IFNA1* was significantly increased after 48 hrs, with a trend for increased expression at 24 and 36 hrs (Figure 7). *TMPRSS2* expression was initially decreased by *Mtb* after 24 hrs of infection but this steadily increased over time, becoming significantly increased

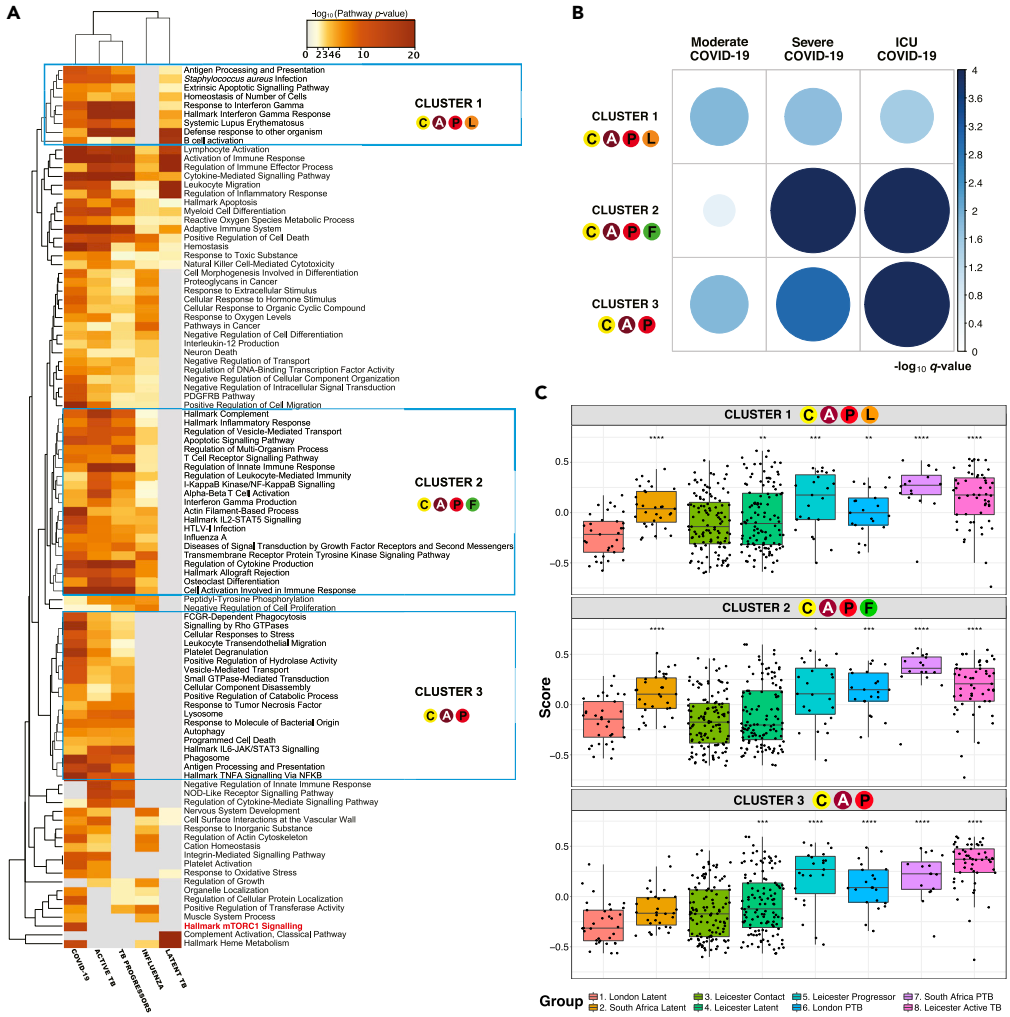

Figure 6. Shared COVID-19 and TB differentially expressed gene clusters correlate with disease severity

(A) Heatmap of the top 100 enriched pathways and three identified gene clusters; circle colors and letters correspond to the groups that formed part of the cluster: C, COVID-19; A, active TB; P, TB progressors; L, latent TB; F, influenza.

(*B*) Bubble plot depicting the enrichment of identified cluster differentially expressed genes (DEGs) by COVID-19 disease severity (see Table S9). The size and shade of the circle correspond to the -$\log_{10}$ *q*-value.

(C) Boxplots of the gene set variation analysis (GSVA) of COVID-19 scores based on the DEGs of each of the three identified clusters. Membership of the groups in the cluster is indicated in the circle appearing in the title of each boxplot. Scores for each signature were compared between each group to the "London Latent" control group using a t-test with Bonferroni correction (see Table S10). Boxplots denote median and 25th to 75th percentiles (boxes) and 10th to 90th percentiles (whiskers). *, p<0·05; **, p<0·005; ***, p<0·0005; ****, p<0·00005.

following 48 hrs of infection. At this time, *ACE2* expression was also significantly induced by *Mtb*, whereas it remained unchanged at earlier time points of infection. The delay in *ACE2* induction is likely a secondary signaling response following MDM exposure to the IFN milieu secreted by infected MDM. As such supernatant was collected from 48hrs *Mtb*-infected and uninfected control MDM, double-filtered to remove *Mtb*, and subsequently used as conditioned media to co-incubate uninfected MDM from the same donors for a further 48 hrs, followed by 72 hrs SARS-CoV-2 infection.

Following SARS-CoV-2 infection, MDM co-incubated in the conditioned media from the *Mtb*-infected MDM exhibited increased SARS-CoV-2 infection as measured by expression of the nucleocapsid gene *N1*, in comparison to MDM not incubated with conditioned media or those incubated in conditioned media from uninfected MDM (p<0.034). Increased SARS-CoV-2 infection most significantly correlated with

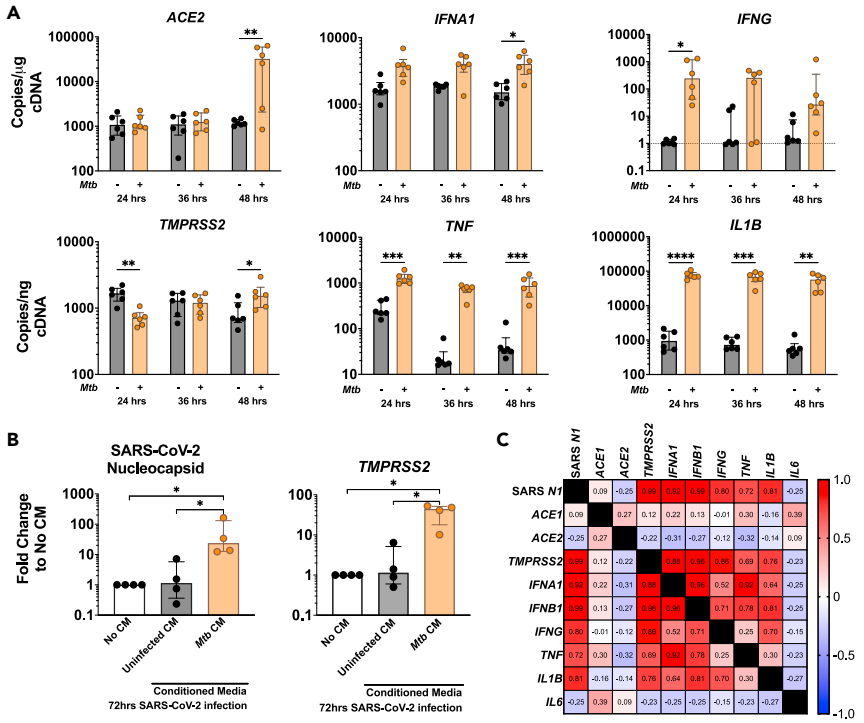

Figure 7. *Mycobacterium tuberculosis* infection increases inflammation and susceptibility to SARS-CoV-2 infection in human macrophages

(A) Expression of pro-inflammatory cytokine genes from monocyte-derived macrophages (MDM), infected with *Mycobacterium tuberculosis* (*Mtb*) for up to 48 hrs, as measured by absolute quantitative RT-PCR, with gene copy number normalized to the housekeeping gene, *RPL13A*; n = 6 donors, paired two-way ANOVA with Sidak's multiple-comparison test.

(*B*) Quantification of SARS-CoV-2 nucleocapsid protein (*N1*) and human serine protease (*TMPRSS2*) gene expression levels from MDM incubated ± conditioned media (CM) from uninfected or *Mtb* infected MDM for 48 h, followed by 72 hrs SARS-CoV-2 infection; n = 4 donors, fold change to no conditioned media treatment was calculated by $2^{-\Delta\Delta Ct}$ relative to the *RPL13A* housekeeping gene, Kruskal-Wallis with Dunn's multiple-comparison test.

(C) Pearson correlation matrix of conditioned media-induced expression fold changes in pro-inflammatory genes and SARS-CoV-2 *N1* from the four donors in *B* across the three experimental conditions. Data in bar plots are represented as median ± interquartile range; *, p<0·05; **, p<0·01; ***, p<0·001; ****, p<0·0001.

increased expression of *TMPRSS2*, *IFNA1*, and *IFNB1* (p<0.00001) as well as *IFNG*, *TNF* and *IL1B* expression at 72 hrs post-SARS-CoV-2 infection (p≤0.006) (Figures 7B and 7C). There was no correlation between SARS-CoV-2 *N1* expression and *ACE1*, *ACE2*, or *IL6* expression in MDM at the same time point (Figure 7C).

DISCUSSION

Substituting TB signatures within the TBSignatureProfiler package with COVID-19 signatures identified from systematic literature review, we profiled 35 identified transcriptional signatures associated with a range of disease severities on 1181 whole blood RNA-seq samples from 853 individuals across the TB disease spectrum. We found that overlapping innate immune cell phenotypes, particularly monocytes, macrophages, and neutrophils, are associated with elevated COVID-19 risk scores in active TB patients and asymptomatic individuals who progress to TB. COVID-19 risk scores were also more elevated in contacts of pulmonary TB cases, compared with extrapulmonary TB contacts. We identified *FCN1*$^{+}$/*SPP1*$^{+}$ macrophage sub-lineages that are enriched in the lungs of severe COVID-19 patients in circulation during active TB. This indicates that critical inflammatory phenotypes which exist in TB patients may exacerbate lung immunopathology upon SARS-CoV-2 infection. Moreover, we observed a substantial overlap in gene ontology enrichment and at a systems level, identifying 12 gene-node interaction networks between COVID-19, active TB, and TB progressors that could serve as disease exacerbation hotspots. Finally, we validate *in vitro* in human MDM that co-culturing in the inflammatory milieu from *Mtb*-infected MDM

increases SARS-CoV-2 infection, associated with increased *TMPRSS2*, type I and II interferon genes, and *TNF* expression.

The enrichment of COVID-19 signatures in individuals with asymptomatic subclinical TB who progress to symptomatic TB over 1–2 years has concerning implications for TB control if induction of immune cell phenotypes common to ATB during co-infection promotes subclinical TB progression. The transcriptional overlap is also likely to decrease specificity of TB RNA-based diagnostic biomarkers, as identified with other seasonal coronavirus co-infections in the recent CORTIS trial, which tested the efficacy of RNA biomarker-guided TB preventive therapy (Scriba et al., 2021). SARS-CoV-2 may therefore pose the biggest threat to ending the TB pandemic since HIV-1 and the modeling increase of 6.8 million extra TB cases in the next five years predicted to be caused by COVID-19 lockdown measures (Stop TB Partnership, 2020a) may underestimate the total increase in TB cases if co-infection leads to increased rates of TB progression.

The most compelling overlaps between COVID-19 signatures and the TB datasets reside in the circulating innate immune cells. Classical monocyte and neutrophil signatures derived from severe COVID-19 patients were associated with the highest COVID-19 risk scores when profiled across the TB spectrum. Circulating monocyte activation status is a determining factor for COVID-19 prognosis, with specific phenotypes leading to poorer outcomes (Zhang et al., 2020). Similar monocyte phenotypes have been detected during TB (Lastrucci et al., 2015). Conversely, adaptive immune cell populations enriched in milder COVID-19 cases were associated with lower scores in ATB and progressors, suggesting coinfected individuals are less likely to experience mild COVID-19.

SARS-CoV-2-infected macrophages are known to accumulate in lungs of patients who died from COVID-19 (Yao et al., 2020b). *FCN1*^{hi} inflammatory-MDMs are abundant in the BALF of severe COVID-19 patients (Liao et al., 2020), indicating their migration to the lungs from the blood, substantiated by an integrative analysis between COVID-19 blood and BALF scRNA-seq samples (Silvin et al., 2020). Here, we show that both the inflammatory *FNC1*^{hi} and *FCN1*^{lo}*SPP1*$^{+}$ sub-lineage signatures had significantly higher WB RNA-seq risk scores in individuals with active and subclinical TB, compared with individuals with non-progressing LTBI. Moreover, our integrative analysis of TB PBMC and COVID-19 BALF scRNA-seq samples showed the presence of these phenotypes in circulation during ATB. *In vitro* we demonstrate that pro-inflammatory human MDM cultured in the inflammatory milieu from *Mtb*-infected MDM are more susceptible to increased SARS-CoV-2 infection. We thus hypothesize that the presence of these sub-lineages in the blood may predispose TB patients to more severe lung disease following SARS-CoV-2 infection.

In support of this hypothesis, scRNA-seq of lung tissue homogenates from TB-HIV coinfected patients has identified upregulation of *ACE2*/*TMPRSS2*-expressing type II pneumocytes (Ziegler et al., 2020). Consistent with *ACE2* being a type I and II interferon-inducible gene, we identified *ACE2* and *TMPRSS2* upregulated in MDM 48 hrs post-*Mtb* infection, following earlier *IFNG* and *IFNA1* induction. Parallel expression of *TNF* by *Mtb*-infected MDM provides an inflammatory environment of synergistic TNF/IFN-γ signaling which has been shown to potentiate PANoptosis and pathogenetic tissue damage in a COVID-19 mouse model, with dual TNF/IFN-γ antibody blocking treatment preventing SARS-CoV-2 mortality in treated mice (Karki et al., 2021). We found that COVID-19 could be distinguished from influenza on the basis of the presence of IFN-γ and TNF response pathways, both of which were highly enriched in ATB and TB progressors. Consistent with this, we also demonstrate upregulation of *IFNA1*, *IFNB1*, *IFNG*, and *TNF* which correlated with increased *TMPRSS2* expression and SARS-CoV-2 replication in MDM co-cultured in *Mtb*-induced conditioned media.

IFN-induced transcriptional signatures were among the most significantly upregulated in severe disease in the studies selected risk profiling (Arunachalam et al., 2020; Huang et al., 2020; Wei et al., 2020; Wilk et al., 2020) and generated high COVID-19 risk scores among ATB cases. Dysregulation of IFN production (Acharya et al., 2020; Hadjadj et al., 2020) and the nature of type I and III IFN responses (location, timing, and duration) in COVID-19 (Broggi et al., 2020; Major et al., 2020) and TB (Cliff et al., 2015) guide disease progression and outcomes. It is therefore plausible that dysregulation of type I IFN responses during SARS-CoV-2 co-infection may also have an impact on subsequent TB disease progression.

At a systems level, shared biological pathways showed a graded enrichment of similar pathways between COVID-19 and active and progressive TB. A PPI-based network analysis identified twelve shared gene-node interaction networks between COVID-19, and active and progressive TB that could serve as disease

exacerbation hotspots (Figures 5C and S7, and Table S10), highlighting shared molecular determinants which could influence clinical outcome during co-infection. The constituent genes are known regulators of pathways that characterize COVID-19 clinical presentation and thus represent potential targets for therapeutic intervention. Consideration of the efficacy of repurposed drugs in treating co-infected patients in low resource settings needs to be considered in future trials, with our meta-analysis providing insight into potential gene therapeutic targets that would require future validation.

We identified enrichment of IL-6-JAK/STAT3 signaling and increased expression of *STAT3*, particularly in COVID-19 patients admitted to the intensive care unit (ICU), and active and progressive TB. Conversely, we found *JAK3* was not significantly differentially expressed in WB in COVID-19 but had very high expression in active and progressive TB and very low expression in influenza. The STAT3 inhibitor ST3-H2A2 and JAK inhibitor tofacitinib, have both improved pulmonary bacterial clearance in chronic TB models (Maiga et al., 2015; Upadhyay et al., 2018). Meta-analysis of JAK inhibitors in COVID-19 found recipients had reduced odds of mortality and ICU admission and increased odds of hospital discharge (Walz et al., 2020). Our results suggest that STAT3 inhibitors may have better efficacy than JAK inhibitors.

STAT3 regulates the activities of nitric oxide synthase and NADPH oxidase (NOX). We found increased expression of the NOX complex gene neutrophil cytosolic factor 1 (*NCF1*) in severe COVID-19 and active/progressive TB. NCF1 activation of NAPDH and subsequent ROS production requires complexation with PAD4, whereas inhibition of PAD4 using simvastatin or GSK484, prevents ROS-mediated neutrophil extracellular trap (NET) formation (Sapey et al., 2019; Zhou et al., 2018). NETs are proposed to contribute to COVID-19 acute respiratory distress syndrome (ARDS) and coagulopathy, with NET inhibitors proposed as COVID-19 therapeutics (Schonrich et al., 2020; Sultana et al., 2020). An alternate NCF1 inhibitor, Apocynin, prevents oxidative stress in diabetic rats (Olukman et al., 2018). Interestingly, metformin, which is commonly used to treat Diabetes Mellitus and proposed as a host-directed therapy for TB, increases ROS gene and *NCF1* expression (Lachmandas et al., 2019). Our results suggest metformin be avoided in TB patients with COVID-19. *CD74* (HLA-DR-Gamma), the receptor for macrophage inhibitory factor 1 (MIF), also increases pulmonary neutrophil infiltration (Takahashi et al., 2009), and ROS production in TB (Das et al., 2013). CD74 can be blocked with either MIF antagonist (ISO-1), MIF inhibitors (vorinostat), or anti-CD74 neutralizing antibodies (Cavalli et al., 2019; Takahashi et al., 2009).

SLC2A3, encoding the glucose uptake transporter GLUT3 and *LCP1* (L-Plastin) are induced during hypoxia by STAT-3-HIF1α signaling and regulate macrophage infiltration (Gerri et al., 2017; Yao et al., 2020a). Glycolytic reprogramming by GLUT3 is also associated with type 2 macrophage polarization and a SLCA23-STAT3 feedback loop promotes STAT3 phosphorylation (Yao et al., 2020a). Anticancer agents vanillin and chaetocin inhibit HIF1α transactivation (Kung et al., 2004; Park et al., 2017), chaetocin also inhibits *STAT3* expression (Yang et al., 2020), and p-STAT3 inhibitor APSTAT3-9R inhibits SLAC2A3 expression (Yao et al., 2020a), suggesting they have a synergistic benefit in amelioration of STAT3-HIF-1α oxidative stress.

Platelet activation increases glycolysis, mitochondrial depolarization, and ROS production leading to platelet apoptosis and thrombosis (Garcia-Souza and Oliveira, 2014). Maintaining platelet homeostasis by balancing mitochondrial oxidative stress is critical to limit coagulopathy (Sapey et al., 2019; Zhou et al., 2018). BCL-6 which inhibits antiapoptotic proteins BCL-XL and BCL-2 was also upregulated in COVID-19 and TB disease states, suggesting cancer therapies targeting BLC-6 (such as RI-BPI)(Cardenas et al., 2017) may possess therapeutic potential. Integrin coactivator Talin-1 (*TLN1*) was also highly expressed in COVID-19, active TB, and TB progressors. Talin-1 plays a critical role in activating thrombosis and neutrophil infiltration via integrin-mediated endothelial transmigration (Garcia-Souza and Oliveira, 2014). Methylation of talin-1 at Lys2454 is required for talin-1 mediated neutrophil infiltration during LPS-induced endotoxemia, which can be blocked with the methyltransferase EZH2 inhibitor GSK126 (Petrich et al., 2007).

In summary, we show for the first time through large scale meta-analysis of available transcriptomic data that COVID-19 and TB disease states overlap at the gene, cell, and systems levels. Genes commonly enriched in COVID-19 and TB illustrate similarities in immunopathogenesis that may exacerbate disease severity during co-infection trigger TB progression and decrease biomarker specificity. Selecting therapeutic targets shared by COVID-19 and TB may have significant utility in treating co-infected patients to

not only reduce COVID-19 disease severity but also prevent potential TB progression. With the emergence of SARS-CoV-2 variants in TB endemic countries showing greater vaccine escape (Fontanet et al., 2021), new therapeutics with efficacy in treating co-infection are critical.

Limitations of the study

Although several of the preprint manuscripts identified at the beginning of our study have since been published in high-impact journals, our COVID-19 signature search was complicated by the limited availability of supplementary data detailing cell cluster markers or DEG lists. Furthermore, the COVID-19 studies performed to date are confined to small numbers of patients in each group that exhibit interindividual variability in immune cell phenotypes. We counteracted this limitation by including signatures from multiple studies for each immune cell population. Although COVID-19 studies originated from France, the US, and China have been included, the ethnic background of all participants is not described and thus may not represent the diversity of immunological responses from all populations with high TB prevalence. We also note that TB exposure has not been described by any of the COVID-19 studies included in the analysis, so concurrent TB infection cannot be excluded.

STAR★METHODS

Detailed methods are provided in the online version of this paper and include the following:

- KEY RESOURCES TABLE
- RESOURCE AVAILABILITY
  - Lead contact
  - Materials availability
  - Data and code availability
- EXPERIMENTAL MODEL AND SUBJECT DETAILS
  - Human blood samples
  - *Mycobacterium tuberculosis* single cell stock generation
  - SARS-CoV-2 stock preparation
  - Monocyte culture
  - Macrophage culture
- METHOD DETAILS
  - Search strategy, selection criteria and data extraction
  - Profiling for COVID-19 risk
  - Single-cell integrative analysis
  - Functional enrichment analysis
  - Protein-protein interaction and gene set enrichment analysis
  - Macrophage infection
  - RT-PCR
- QUANTIFICATION AND STATISTICAL ANALYSIS

SUPPLEMENTAL INFORMATION

Supplemental information can be found online at https://doi.org/10.1016/j.isci.2022.104464.

ACKNOWLEDGMENTS

The authors thank Coussens Lab members for feedback and the Pellegrini Lab at the Walter and Eliza Hall Institute of Medical Research (WEHI) for providing Vero cells and input into SARS-CoV-2 assays. D.S. and W.V. are supported by WEHI. A. is supported by AXA research Fund (25776); National Research Foundation, South Africa (NRF; UID8829) and the Medical Research Council of South Africa (SAMRC; SHIP-02-2013). N.P. is supported by the Carnegie Foundation and Australia Awards Africa Postdoctoral Fellowship (DFAT). X.W. is supported by the National Institutes of Health (NIH; R21AI154387). W.E.J. is funded by CRDF Global (DAA3-19-65672-1) and the NIH (U19AI111276, U01CA220413, R01GM127430, R21AI154387). A.K.C. is funded by WEHI, Jenny Tatchell, SAMRC (SHIP-02-2013), NIH (U19AI111276) and the Australian Respiratory Council. Graphical abstract was created with BioRender.com.

AUTHOR CONTRIBUTIONS

A.K.C., D.S., and A. conceived and designed the study. D.S. and A. contributed equally to the data analysis and A.K.C. supervised the analysis. Systematic review of COVID-19 manuscripts and identification of TB datasets was performed by D.S., X.W., and A. The curatedTBData package used to obtain the TB transcriptomic data and associated patient metadata was created by X.W. and W.E.J. COVID-19 signature risk profiling and scRNA-seq analysis was performed by D.S. with input from W.E.J., who developed the TBSignatureProfiler package with colleagues. SARS-CoV-2 stocks and assays were established by C.A. *Mtb* stock generation, MDM infections, and RT-PCR were performed by N.P., D.S. and W.V. Functional enrichment analysis and GSEA were performed by A. D.S, A., and A.K.C. prepared the manuscript. All authors contributed editorial input and approved the manuscript submission.

DECLARATION OF INTERESTS

The authors declare no competing interests.

INCLUSION AND DIVERSITY

We worked to ensure gender balance in the recruitment of human subjects. One or more of the authors of this paper self-identifies as an underrepresented ethnic minority in science. One or more of the authors of this paper self-identifies as a member of the LGBTQ+ community. One or more of the authors of this paper received support from a program designed to increase minority representation in science.

Received: March 13, 2021
Revised: January 14, 2022
Accepted: May 18, 2022
Published: June 17, 2022

REFERENCES

Acharya, D., Liu, G., and Gack, M.U. (2020). Dysregulation of type I interferon responses in COVID-19. Nat. Rev. Immunol. *20*, 397–398. https://doi.org/10.1038/s41577-020-0346-x.

Arunachalam, P.S., Wimmers, F., Mok, C.K.P., Perera, R.A.P.M., Scott, M., Hagan, T., Sigal, N., Feng, Y., Bristow, L., Tak-Yin Tsang, O., et al. (2020). Systems biological assessment of immunity to mild versus severe COVID-19 infection in humans. Science *369*, 1210–1220. https://doi.org/10.1126/science.abc6261.

Bader, G.D., and Hogue, C.W.V. (2003). An automated method for finding molecular complexes in large protein interaction networks. BMC Bioinf. *4*, 2. https://doi.org/10.1186/1471-2105-4-2.

Boulle, A., Davies, M.A., Hussey, H., Ismail, M., Morden, E., Vundle, Z., Zweigenthal, V., Mahomed, H., Paleker, M., Pienaar, D., et al. (2021). Risk factors for COVID-19 death in a population cohort study from the Western Cape Province, South Africa. Clin. Infect. Dis. *73*, e2005–e2015.

Broggi, A., Ghosh, S., Sposito, B., Spreafico, R., Balzarini, F., Lo Cascio, A., Clementi, N., De Santis, M., Mancini, N., Granucci, F., et al. (2020). Type III interferons disrupt the lung epithelial barrier upon viral recognition. Science *369*, 706–712. https://doi.org/10.1126/science.abc3545.

Cai, Y., Dai, Y., Wang, Y., Yang, Q., Guo, J., Wei, C., Chen, W., Huang, H., Zhu, J., Zhang, C., et al. (2020). Single-cell transcriptomics of blood reveals a natural killer cell subset depletion in tuberculosis. EBioMedicine *53*, 102686. https://doi.org/10.1016/j.ebiom.2020.102686.

Cardenas, M.G., Oswald, E., Yu, W., Xue, F., MacKerell, A.D., Jr., and Melnick, A.M. (2017). The expanding role of the BCL6 oncoprotein as a cancer therapeutic target. Clin. Cancer Res. *23*, 885–893. https://doi.org/10.1158/1078-0432.ccr-16-2071.

Cavalli, E., Mazzon, E., Mammana, S., Basile, M.S., Lombardo, S.D., Mangano, K., Bramanti, P., Nicoletti, F., Fagone, P., and Petralia, M.C. (2019). Overexpression of macrophage migration inhibitory factor and its homologue D-dopachrome tautomerase as negative prognostic factor in neuroblastoma. Brain Sci. *9*, 284. https://doi.org/10.3390/brainsci9100284.

Cliff, J.M., Kaufmann, S.H.E., McShane, H., van Helden, P., and O'Garra, A. (2015). The human immune response to tuberculosis and its treatment: a view from the blood. Immunol. Rev. *264*, 88–102. https://doi.org/10.1111/imr.12269.

Das, R., Koo, M.S., Kim, B.H., Jacob, S.T., Subbian, S., Yao, J., Leng, L., Levy, R., Murchison, C., Burman, W.J., et al. (2013). Macrophage migration inhibitory factor (MIF) is a critical mediator of the innate immune response to Mycobacterium tuberculosis. Proc. Natl. Acad. Sci. U S A *110*, E2997–E3006. https://doi.org/10.1073/pnas.1301128110.

Dunning, J., Blankley, S., Hoang, L.T., Cox, M., Graham, C.M., James, P.L., Bloom, C.I., Chaussabel, D., Banchereau, J., Brett, S.J., et al. (2018). Progression of whole-blood transcriptional signatures from interferon-induced to neutrophil-associated patterns in severe influenza. Nat. Immunol. *19*, 625–635. https://doi.org/10.1038/s41590-018-0111-5.

Fontanet, A., Autran, B., Lina, B., Kieny, M.P., Karim, S.S.A., and Sridhar, D. (2021). SARS-CoV-2 variants and ending the COVID-19 pandemic. Lancet *397*, 952–954. https://doi.org/10.1016/s0140-6736(21)00370-6.

Garcia-Souza, L.F., and Oliveira, M.F. (2014). Mitochondria: biological roles in platelet physiology and pathology. Int. J. Biochem. Cell Biol. *50*, 156–160. https://doi.org/10.1016/j.biocel.2014.02.015.

Gerri, C., Marin-Juez, R., Marass, M., Marks, A., Maischein, H.M., and Stainier, D.Y.R. (2017). Hif-1α regulates macrophage-endothelial interactions during blood vessel development in zebrafish. Nat. Commun. *8*, 15492. https://doi.org/10.1038/ncomms15492.

Hadjadj, J., Yatim, N., Barnabei, L., Corneau, A., Boussier, J., Smith, N., Péré, H., Charbit, B., Bondet, V., Chenevier-Gobeaux, C., et al. (2020). Impaired type I interferon activity and inflammatory responses in severe COVID-19 patients. Science *369*, 718–724. https://doi.org/10.1126/science.abc6027.

Hänzelmann, S., Castelo, R., and Guinney, J. (2013). GSVA: gene set variation analysis for microarray and RNA-Seq data. BMC Bioinf. *14*, 7. https://doi.org/10.1186/1471-2105-14-7.

Hasan, M.N., Haider, N., Stigler, F.L., Khan, R.A., McCoy, D., Zumla, A., Kock, R.A., and Uddin, M.J. (2021). The global case-fatality rate of COVID-19 has been declining since may 2020. Am. J. Trop.

Med. Hyg. *104*, 2176–2184. https://doi.org/10.4269/ajtmh.20-1496.

Haynes, W. (2013). Benjamini–hochberg method. In Encyclopedia of Systems Biology, W. Dubitzky, O. Wolkenhauer, K.-H. Cho, and H. Yokota, eds. (New York, NY: Springer New York), p. 78. https://doi.org/10.1007/978-1-4419-9863-7_1215.

Houben, R.M.G.J., and Dodd, P.J. (2016). The global burden of latent tuberculosis infection: a Re-estimation using mathematical modelling. PLoS Med. *13*, e1002152. https://doi.org/10.1371/journal.pmed.1002152.

Huang, L., Shi, Y., Gong, B., Jiang, L., Liu, X., Yang, J., Tang, J., You, C., Jiang, Q., Long, B., et al. (2020). Blood single cell immune profiling reveals the interferon-MAPK pathway mediated adaptive immune response for COVID-19. Preprint at medRxiv. https://doi.org/10.1101/2020.03.15.20033472.

Jenkins, D., Zhao, Y., Johnson, W.E., Odom, A., and Love, C. (2020). TBSignatureProfiler: Profile RA-Seq Data Using TB Pathway Signatures. https://github.com/compbiomed/TBSignatureProfiler.

Karki, R., Sharma, B.R., Tuladhar, S., Williams, E.P., Zalduondo, L., Samir, P., Zheng, M., Sundaram, B., Banoth, B., Malireddi, R.S., et al. (2021). Synergism of TNF-alpha and IFN-gamma triggers inflammatory cell death, tissue damage, and mortality in SARS-CoV-2 infection and cytokine shock syndromes. Cell *184*, 149–168.e17. https://doi.org/10.1016/j.cell.2020.11.025.

Kung, A.L., Zabludoff, S.D., France, D.S., Freedman, S.J., Tanner, E.A., Vieira, A., Cornell-Kennon, S., Lee, J., Wang, B., Wang, J., et al. (2004). Small molecule blockade of transcriptional coactivation of the hypoxia-inducible factor pathway. Cancer Cell *6*, 33–43. https://doi.org/10.1016/j.ccr.2004.06.009.

Lachmandas, E., Eckold, C., Bohme, J., Koeken, V.A.C.M., Marzuki, M.B., Blok, B., Arts, R.J.W., Chen, J., Teng, K.W.W., Ratter, J., et al. (2019). Metformin alters human host responses to Mycobacterium tuberculosis in healthy subjects. J. Infect. Dis. *220*, 139–150. https://doi.org/10.1093/infdis/jiz064.

Lastrucci, C., Bénard, A., Balboa, L., Pingris, K., Souriant, S., Poincloux, R., Al Saati, T., Rasolofo, V., González-Montaner, P., Inwentarz, S., et al. (2015). Tuberculosis is associated with expansion of a motile, permissive and immunomodulatory CD16+ monocyte population via the IL-10/STAT3 axis. Cell Res. *25*, 1333–1351. https://doi.org/10.1038/cr.2015.123.

Li, T., Wernersson, R., Hansen, R.B., Horn, H., Mercer, J., Slodkowicz, G., Workman, C.T., Rigina, O., Rapacki, K., Stærfeldt, H.H., et al. (2017). A scored human protein-protein interaction network to catalyze genomic interpretation. Nat. Methods *14*, 61–64. https://doi.org/10.1038/nmeth.4083.

Liao, M., Liu, Y., Yuan, J., Wen, Y., Xu, G., Zhao, J., Cheng, L., Li, J., Wang, X., Wang, F., et al. (2020). Single-cell landscape of bronchoalveolar immune cells in patients with COVID-19. Nat. Med. *26*, 842–844. https://doi.org/10.1038/s41591-020-0901-9.

Liu, Y., Bi, L., Chen, Y., Wang, Y., Fleming, J., Yu, Y., Gu, Y., Liu, C., Fan, L., Wang, X., et al. (2020). Active or latent tuberculosis increases susceptibility to COVID-19 and disease severity. Preprint at medRxiv. https://doi.org/10.1101/2020.03.10.20033795.

Maiga, M., Ahidjo, B.A., Maiga, M.C., Cheung, L., Pelly, S., Lun, S., Bougoudogo, F., and Bishai, W.R. (2015). Efficacy of adjunctive tofacitinib therapy in mouse models of tuberculosis. EBioMedicine *2*, 868–873. https://doi.org/10.1016/j.ebiom.2015.07.014.

Major, J., Crotta, S., Llorian, M., McCabe, T.M., Gad, H.H., Priestnall, S.L., Hartmann, R., and Wack, A. (2020). Type I and III interferons disrupt lung epithelial repair during recovery from viral infection. Science *369*, 712–717. https://doi.org/10.1126/science.abc2061.

Motta, I., Centis, R., D'Ambrosio, L., García-García, J.M., Goletti, D., Gualano, G., Lipani, F., Palmieri, F., Sánchez-Montalvá, A., Pontali, E., et al. (2020). Tuberculosis, COVID-19 and migrants: preliminary analysis of deaths occurring in 69 patients from two cohorts. Pulmonology *26*, 233–240. https://doi.org/10.1016/j.pulmoe.2020.05.002.

Olukman, M., Onal, A., Celenk, F.G., Uyanikgil, Y., Cavusoglu, T., Duzenli, N., and Ulker, S. (2018). Treatment with NADPH oxidase inhibitor apocynin alleviates diabetic neuropathic pain in rats. Neural Regen. Res. *13*, 1657–1664. https://doi.org/10.4103/1673-5374.232530.

Oughtred, R., Stark, C., Breitkreutz, B.J., Rust, J., Boucher, L., Chang, C., Kolas, N., O'Donnell, L., Leung, G., McAdam, R., et al. (2019). The BioGRID interaction database: 2019 update. Nucleic Acids Res. *47*, 529–541. https://doi.org/10.1093/nar/gky1079.

Park, E.J., Lee, Y.M., Oh, T.I., Kim, B.M., Lim, B.O., and Lim, J.H. (2017). Vanillin suppresses cell motility by inhibiting STAT3-mediated HIF-1α mRNA expression in malignant melanoma cells. Int. J. Mol. Sci. *18*, 532. https://doi.org/10.3390/ijms18030532.

Petrich, B.G., Marchese, P., Ruggeri, Z.M., Spiess, S., Weichert, R.A., Ye, F., Tiedt, R., Skoda, R.C., Monkley, S.J., Critchley, D.R., and Ginsberg, M.H. (2007). Talin is required for integrin-mediated platelet function in hemostasis and thrombosis. J. Exp. Med. *204*, 3103–3111. https://doi.org/10.1084/jem.20071800.

R Core Team (2020). R: A Language and Environment for Statistical Computing.

Ramakrishnan, M.A. (2016). Determination of 50% endpoint titer using a simple formula. World J. Virol. *5*, 85–86. https://doi.org/10.5501/wjv.v5.i2.85.

Ritchie, M.E., Phipson, B., Wu, D., Hu, Y., Law, C.W., Shi, W., and Smyth, G.K. (2015). Limma powers differential expression analyses for RNA-sequencing and microarray studies. Nucleic Acids Res. *43*, e47. https://doi.org/10.1093/nar/gkv007.

Sapey, E., Patel, J.M., Greenwood, H., Walton, G.M., Grudzinska, F., Parekh, D., Mahida, R.Y., Dancer, R.C.A., Lugg, S.T., Howells, P.A., et al. (2019). Simvastatin improves neutrophil function and clinical outcomes in pneumonia. A pilot randomized controlled clinical trial. Am. J. Respir. Crit. Care Med. *200*, 1282–1293. https://doi.org/10.1164/rccm.201812-2328oc.

Satija, R., Farrell, J.A., Gennert, D., Schier, A.F., and Regev, A. (2015). Spatial reconstruction of single-cell gene expression data. Nat. Biotechnol. *33*, 495–502. https://doi.org/10.1038/nbt.3192.

Schonrich, G., Raftery, M.J., and Samstag, Y. (2020). Devilishly radical NETwork in COVID-19: oxidative stress, neutrophil extracellular traps (NETs), and T cell suppression. Adv. Biol. Regul. *77*, 100741. https://doi.org/10.1016/j.jbior.2020.100741.

Scriba, T.J., Fiore-Gartland, A., Penn-Nicholson, A., Mulenga, H., Kimbung Mbandi, S., Borate, B., Mendelsohn, S.C., Hadley, K., Hikuam, C., Kaskar, M., et al.; CORTIS-01 Study Team (2021). Biomarker-guided tuberculosis preventive therapy (CORTIS): a randomised controlled trial. Lancet Infect. Dis. *21*, 354–365. https://doi.org/10.1016/S1473-3099(20)30914-2.

Shannon, P., Markiel, A., Ozier, O., Baliga, N.S., Wang, J.T., Ramage, D., Amin, N., Schwikowski, B., and Ideker, T. (2003). Cytoscape: a software environment for integrated models of biomolecular interaction networks. Genome Res. *13*, 2498–2504. https://doi.org/10.1101/gr.1239303.

Shao, X., Liao, J., Lu, X., Xue, R., Ai, N., and Fan, X. (2020). scCATCH: automatic annotation on cell types of clusters from single-cell RNA sequencing data. iScience *23*, 100882. https://doi.org/10.1016/j.isci.2020.100882.

Silvin, A., Chapuis, N., Dunsmore, G., Goubet, A.G., Dubuisson, A., Derosa, L., Almire, C., Hénon, C., Kosmider, O., Droin, N., et al. (2020). Elevated calprotectin and abnormal myeloid cell subsets discriminate severe from mild COVID-19. Cell *182*, 1401–1418.e18. https://doi.org/10.1016/j.cell.2020.08.002.

Singhania, A., Verma, R., Graham, C.M., Lee, J., Tran, T., Richardson, M., Lecine, P., Leissner, P., Berry, M.P.R., Wilkinson, R.J., et al. (2018). A modular transcriptional signature identifies phenotypic heterogeneity of human tuberculosis infection. Nat. Commun. *9*, 2308. https://doi.org/10.1038/s41467-018-04579-w.

Stop TB Partnership (2020a). The Potential Impact of the COVID-19 Response on Tuberculosis in High-Burden Countries: A Modelling Analysis. http://www.stoptb.org/assets/documents/news/Modeling%20Report_1%20May%202020_FINAL.pdf.

Stop TB Partnership. (2020b). We Did a Rapid Assessment: The TB Response Is Heavily Impacted by the COIVD-19 Pandemic. http://stoptb.org/news/stories/2020/ns20_014.html.

Stuart, T., Butler, A., Hoffman, P., Hafemeister, C., Papalexi, E., Mauck, W.M., III, Hao, Y., Stoeckius, M., Smibert, P., and Satija, R. (2019). Comprehensive integration of single-cell data. Cell *177*, 1888–1902.e21. https://doi.org/10.1016/j.cell.2019.05.031.

Subramanian, A., Tamayo, P., Mootha, V.K., Mukherjee, S., Ebert, B.L., Gillette, M.A., Paulovich, A., Pomeroy, S.L., Golub, T.R., Lander, E.S., et al. (2005). Gene set enrichment analysis: a

knowledge-based approach for interpreting genome-wide expression profiles. Proc. Natl. Acad. Sci. U S A *102*, 15545–15550. https://doi.org/10.1073/pnas.0506580102.

Suliman, S., Thompson, E.G., Sutherland, J., Weiner, J., 3rd, Ota, M.O.C., Shankar, S., Penn-Nicholson, A., Thiel, B., Erasmus, M., Maertzdorf, J., et al. (2018). Four-gene pan-african blood signature predicts progression to tuberculosis. Am. J. Respir. Crit. Care Med. *197*, 1198–1208. https://doi.org/10.1164/rccm.201711-2340OC.

Sultana, J., Crisafulli, S., Gabbay, F., Lynn, E., Shakir, S., and Trifiro, G. (2020). Challenges for drug repurposing in the COVID-19 pandemic era. Front. Pharmacol. *11*, 588654. https://doi.org/10.3389/fphar.2020.588654.

Tadolini, M., Codecasa, L.R., García-García, J.M., Blanc, F.X., Borisov, S., Alffenaar, J.W., Andréjak, C., Bachez, P., Bart, P.A., Belilovski, E., et al. (2020). Active tuberculosis, sequelae and COVID-19 co-infection: first cohort of 49 cases. Eur. Respir. J. *56*, 2001398. https://doi.org/10.1183/13993003.01398-2020.

Takahashi, K., Koga, K., Linge, H.M., Zhang, Y., Lin, X., Metz, C.N., Al-Abed, Y., Ojamaa, K., and Miller, E.J. (2009). Macrophage CD74 contributes to MIF-induced pulmonary inflammation. Respir. Res. *10*, 33. https://doi.org/10.1186/1465-9921-10-33.

The TB/COVID Global Study Group (2021). Tuberculosis and COVID-19 co-infection: description of the global cohort. Eur. Respir. J. 2102538.

Türei, D., Korcsmáros, T., and Saez-Rodriguez, J. (2016). OmniPath: guidelines and gateway for literature-curated signaling pathway resources. Nat. Methods *13*, 966–967. https://doi.org/10.1038/nmeth.4077.

Upadhyay, R., Sanchez-Hidalgo, A., Wilusz, C.J., Lenaerts, A.J., Arab, J., Yeh, J., Stefanisko, K., Tarasova, N.I., and Gonzalez-Juarrero, M. (2018). Host directed therapy for chronic tuberculosis via intrapulmonary delivery of aerosolized peptide inhibitors targeting the IL-10-STAT3 pathway. Sci. Rep. *8*, 16610. https://doi.org/10.1038/s41598-018-35023-0.

van Enst, W.A., Ochodo, E., Scholten, R.J., Hooft, L., and Leeflang, M.M. (2014). Investigation of publication bias in meta-analyses of diagnostic test accuracy: a meta-epidemiological study. BMC Med. Res. Methodol. *14*, 70. https://doi.org/10.1186/1471-2288-14-70.

Viechtbauer, W. (2010). Conducting meta-analyses in R with the metafor package. J. Stat. Software *36*, 1–48. https://doi.org/10.18637/jss.v036.i03.

Walz, L., Cohen, A.J., Rebaza, A.P., Vanchieri, J., Slade, M.D., Dela Cruz, C.S., and Sharma, L. (2020). Janus kinase-inhibitor and type I interferon ability to produce favorable clinical outcomes in COVID-19 patients: a systematic review and meta-analysis. Preprint at medRxiv. https://doi.org/10.1101/2020.08.10.20172189.

Wang, X. (2020). curatedTBData: Curation of Existing 42 Tuberculosis Transcriptomic Studies. R package version 0.1.0. https://github.com/compbiomed/curatedTBData.

Wei, L., Ming, S., Zou, B., Wu, Y., Hong, Z., Li, Z., Zheng, X., Huang, M., Luo, L., Liang, J., et al. (2020). Viral invasion and type I interferon response characterize the immunophenotypes during COVID-19 infection. SSRN. https://doi.org/10.2139/ssrn.3555695.

Wen, W., Su, W., Tang, H., Le, W., Zhang, X., Zheng, Y., Liu, X., Xie, L., Li, J., Ye, J., et al. (2020). Author Correction: immune cell profiling of COVID-19 patients in the recovery stage by single-cell sequencing. Cell Discov. *6*, 41. https://doi.org/10.1038/s41421-020-00187-5.

Wilk, A.J., Rustagi, A., Zhao, N.Q., Roque, J., Martínez-Colón, G.J., McKechnie, J.L., Ivison, G.T., Ranganath, T., Vergara, R., Hollis, T., et al. (2020). A single-cell atlas of the peripheral immune response in patients with severe COVID-19. Nat. Med. *26*, 1070–1076. https://doi.org/10.1038/s41591-020-0944-y.

World Health Organization (2021a). Global Tuberculosis Report 2021. https://www.who.int/teams/global-tuberculosis-programme/tb-reports.

World Health Organisation (2021b). The True Death Toll of COVID-19: Estimating Global Excess Mortality. https://www.who.int/data/stories/the-true-death-toll-of-covid-19-estimating-global-excess-mortality.

Xiong, Y., Liu, Y., Cao, L., Wang, D., Guo, M., Jiang, A., Guo, D., Hu, W., Yang, J., Tang, Z., et al. (2020). Transcriptomic characteristics of bronchoalveolar lavage fluid and peripheral blood mononuclear cells in COVID-19 patients. Emerg. Microb. Infect. *9*, 761–770. https://doi.org/10.1080/22221751.2020.1747363.

Yang, Z., Wang, H., Zhang, N., Xing, T., Zhang, W., Wang, G., Li, C., and Yu, C. (2020). Chaetocin abrogates the self-renewal of bladder cancer stem cells via the suppression of the KMT1A-GATA3-STAT3 circuit. Front. Cell Dev. Biol. *8*, 424. https://doi.org/10.3389/fcell.2020.00424.

Yao, X., He, Z., Qin, C., Deng, X., Bai, L., Li, G., and Shi, J. (2020a). SLC2A3 promotes macrophage infiltration by glycolysis reprogramming in gastric cancer. Cancer Cell Int. *20*, 503. https://doi.org/10.1186/s12935-020-01599-9.

Yao, X.H., Li, T.Y., He, Z.C., Ping, Y.F., Liu, H.W., Yu, S.C., Mou, H.M., Wang, L.H., Zhang, H.R., Fu, W.J., et al. (2020b). A pathological report of three COVID-19 cases by minimal invasive autopsies. Zhonghua Bing Li Xue Za Zhi *49*, 411–417. https://doi.org/10.3760/cma.j.cn112151-20200312-00193.

Zak, D.E., Penn-Nicholson, A., Scriba, T.J., Thompson, E., Suliman, S., Amon, L.M., Mahomed, H., Erasmus, M., Whatney, W., Hussey, G.D., et al. (2016). A blood RNA signature for tuberculosis disease risk: a prospective cohort study. Lancet *387*, 2312–2322. https://doi.org/10.1016/S0140-6736(15)01316-1.

Zhang, D., Guo, R., Lei, L., Liu, H., Wang, Y., Wang, Y., Dai, T., Zhang, T., Lai, Y., Wang, J., et al. (2020). COVID-19 infection induces readily detectable morphological and inflammation-related phenotypic changes in peripheral blood monocytes, the severity of which correlate with patient outcome. Preprint at medRxiv. https://doi.org/10.1101/2020.03.24.20042655.

Zhou, Y., An, L.L., Chaerkady, R., Mittereder, N., Clarke, L., Cohen, T.S., Chen, B., Hess, S., Sims, G.P., and Mustelin, T. (2018). Evidence for a direct link between PAD4-mediated citrullination and the oxidative burst in human neutrophils. Sci. Rep. *8*, 15228. https://doi.org/10.1038/s41598-018-33385-z.

Zhou, Y., Zhou, B., Pache, L., Chang, M., Khodabakhshi, A.H., Tanaseichuk, O., Benner, C., and Chanda, S.K. (2019). Metascape provides a biologist-oriented resource for the analysis of systems-level datasets. Nat. Commun. *10*, 1523. https://doi.org/10.1038/s41467-019-09234-6.

Ziegler, C.G.K., Allon, S.J., Nyquist, S.K., Mbano, I.M., Miao, V.N., Tzouanas, C.N., Cao, Y., Yousif, A.S., Bals, J., Hauser, B.M., et al. (2020). SARS-CoV-2 receptor ACE2 is an interferon-stimulated gene in human airway epithelial cells and is detected in specific cell subsets across tissues. Cell *181*, 1016–1035. https://doi.org/10.1016/j.cell.2020.04.035.

Zumla, A., Marais, B.J., McHugh, T.D., Maeurer, M., Zumla, A., Kapata, N., Ntoumi, F., Chanda-Kapata, P., Mfinanga, S., Centis, R., et al. (2020). COVID-19 and tuberculosis-threats and opportunities. Int. J. Tubercul. Lung Dis. *24*, 757–760. https://doi.org/10.5588/ijtld.20.0387.

STAR★METHODS

KEY RESOURCES TABLE

REAGENT or RESOURCE	SOURCE	IDENTIFIER
Bacterial and virus strains		
SARS-CoV-2	Peter Doherty Institute	VIC001
Mycobacterium tuberculosis lineage 2 clinical isolate	Wellcome Centre for Infectious Disease Research in Africa	MRC57
Biological samples		
Human adult blood	Australian Red Cross Lifeblood	WEHI HREC #18_09LR; ARCL HREC #18-11VIC-06, #21-01VIC-02
Chemicals, peptides, and recombinant proteins		
Difco™ Middlebrook 7H9 broth	Becton Dickinson	Cat#271310
Middlebrook ADC enrichment	Becton Dickinson	Cat#211887
Tween 80	Sigma-Aldrich	Cat#P1754
Dulbecco's phosphate-buffered saline	ThermoFisher	Cat#14190144
Glycerol	ThermoFisher	Cat#17904
Difco™ Middlebrook 7H10 agar	Becton Dickinson	Cat#262710
Dulbecco's Modified Eagle Medium	ThermoFisher	Cat#12491015
Lymphoprep™	StemCell Technologies	Cat#07851
RPMI 1640 media	ThermoFisher	Cat#11875093
L-glutamine	Gibco	Cat#25030081
Sodium pyruvate	Gibco	Cat#11360070
Human AB serum	Sigma-Aldrich	Cat#H6914
Human GM-CSF	Miltenyi Biotec	Cat#130-093-864
Accutase	Sigma-Aldrich	Cat#A6964
TRIzol reagent	Life Technologies	Cat#15596026
Trypsin, TPCK Treated	ThermoFisher	Cat#20233
Chloroform – isoamyl alcohol mixture	Sigma-Aldrich	Cat#25666
2-Propanol	Sigma-Aldrich	Cat#I9516
Sodium acetate	Sigma-Aldrich	Cat#S2889
Linear Acrylamide	Life Technologies	Cat#AM9520
Ethanol	Sigma-Aldrich	Cat#E7023
Critical commercial assays		
High Capacity cDNA synthesis kit	Applied Biosystems	Cat#4368814
Fast SYBR™ Green Master Mix	Applied Biosystems	Cat#4385610
2019-nCoV RUO kit	Integrated DNA Technologies	Cat#1006713
iTaq Universal Probes One-Step kit	Bio-Rad	Cat#1725140
CD14 MicroBeads, human	Miltenyi Biotec	Cat#130-050-201
QuadroMACS™ Starting Kit (LS)	Miltenyi Biotec	Cat#130-091-051
Deposited data		
WB influenza microarray dataset	(Dunning et al., 2018)	GEO: GSE111368
COVID-19 BALF scRNA-seq dataset	(Liao et al., 2020)	GEO: GSE145926

(*Continued on next page*)

Continued

REAGENT or RESOURCE	SOURCE	IDENTIFIER
TB PBMC scRNA-seq dataset	(Cai et al., 2020)	SRA: SRR11038989, SRR11038990, SRR11038991, SRR11038992, SRR11038993, SRR11038994, SRR11038995
Leicester TB WB RNA-seq dataset	(Singhania et al., 2018)	GEO: GSE107994
Adolescent cohort study WB RNA-seq dataset	(Zak et al., 2016)	GEO: GSE79362
Grand Challenges 6 WB RNA-seq dataset	(Suliman et al., 2018)	GEO: GSE94438
COVID-19, bulk RNA-seq PBMCs dataset	(Arunachalam et al., 2020)	GEO: GSE152418
Experimental models: Cell lines		
Vero (CCL-81)	ATCC	ATCC CCL81
Oligonucleotides		
Primer: *ACE1* forward: GACCTGGTGACTGATGAGGCTG	This paper	N/A
Primer: *ACE1* reverse: CTTGCTGGTCTCTGTGGTGATG	This paper	N/A
Primer: *ACE2* forward: CAAAATGGGTCTTCAGTGCTCTC	This paper	N/A
Primer: *ACE2* reverse: CAAGTAATAAGC ATTCTTGTGGATTATC	This paper	N/A
Primer: *IFNA1* forward: AATGGCACAAATGGGAAGAATC	This paper	N/A
Primer: *IFNA1* reverse: CTGAAGAGATTG AAGGTCTGCTG	This paper	N/A
Primer: *IFNB1* forward: ACAACAGGTAGTAGGCGACAC	This paper	N/A
Primer: *IFNB1* reverse: GTGGAGAAGCA CAACAGGAGAG	This paper	N/A
Primer: *IFNG* forward: TGTGGAGACCATCAAGGAAGAC	This paper	N/A
Primer: *IFNG* reverse: GACATTCAAGTCAG TTACCGAATAATTAG	This paper	N/A
Primer: *IL1B* forward: CTGATGGCCCTA AAACAGATGAAG	This paper	N/A
Primer: *IL1B* reverse: AACAACTGACGCGGCCTG	This paper	N/A
Primer: *IL6* forward: AGACAGCCACTCACCTCTTCAG	This paper	N/A
Primer: *IL6* reverse: AGCATCCATCTTTTTCAGCCATC	This paper	N/A
Primer: *RPL13A* forward: CCGGTAGTGGATCTTGGCT	This paper	N/A
Primer: *RPL13A* forward: GAAAAAGCGGATGGTGGTTC	This paper	N/A
Primer: *TMPRSS2* forward: GAGAAAGGG AAGACCTCAGAAGT	This paper	N/A
Primer: *TMPRSS2* reverse: ACCCTGGCAAGAATCGAC	This paper	N/A
Primer: *TNF* forward: CAGGCAGTCAGATCATCTTCTCG	This paper	N/A
Primer: *TNF* reverse: CTCTCAGCTCCACGCCATTG	This paper	N/A
Software and algorithms		
Original code	This paper, GitHub	https://github.com/sheerind-wehi/CRM_COVID-TB
RStudio (v4.0.2)	RStudio Inc.	https://www.rstudio.com/
TBSignatureProfiler (v1.6.0)	(Jenkins et al., 2020)	https://bioconductor.org/packages/release/bioc/html/TBSignatureProfiler.html
metafor (v3.0.2)	(Viechtbauer, 2010)	https://metafor-project.org/doku.php
curatedTBData (v1.0.0)	(Wang, 2020)	https://bioconductor.org/packages/release/data/experiment/html/curatedTBData.html
CellRanger (v4.0.0)	10x Genomics	https://support.10xgenomics.com/single-cell-gene-expression/software/pipelines/latest/installation

(*Continued on next page*)

Continued

REAGENT or RESOURCE	SOURCE	IDENTIFIER
Seurat (v4.0.0)	(Stuart et al., 2019)	https://satijalab.org/seurat/
scCatch (v3.0.0)	(Shao et al., 2020)	https://github.com/ZJUFanLab/scCATCH
limma (v3.50.3)	(Ritchie et al., 2015)	https://bioconductor.org/packages/release/bioc/html/limma.html
Metascape (v3.5.0)	(Zhou et al., 2019)	https://metascape.org/gp/index.html#/main/step1
MCODE (v2.0.0)	(Bader and Hogue, 2003)	ftp://ftp.mshri.on.ca/pub/BIND/Tools/MCODE
Cytoscape (v3.9.1)	(Shannon et al., 2003)	https://cytoscape.org/index.html
Other		
Corning® T25 flasks	Sigma-Aldrich	Cat#CLS430639
Falcon 50 mL conical centrifuge tubes	Fischer Scientific	Cat#14-432-22
Glass beads 2 mm	Sigma-Aldrich	Cat#Z273627
Nunc™ MicroWell™ 96-Well, Nunclon Delta-Treated, Flat-Bottom Microplate	ThermoFisher	Cat#161093
Nunc® CryoTubes®	Sigma-Aldrich	Cat#Z763659
96 Well Round (U) Bottom Plate	ThermoFisher	Cat#143761
Corning® 96-well plate 0.2 PVDF filter membrane	Sigma-Aldrich	Cat#CLS3508
Phasemaker™ Tubes	Life Technologies	Cat#A33248

RESOURCE AVAILABILITY

Lead contact

Further information and requests for resources should be directed to and will be fulfilled by the Lead contact, A/Prof Anna Coussens (coussens.a@wehi.edu.au).

Materials availability

This study did not generate unique reagents.

Data and code availability

- RNA-seq data and associated patient metadata are publicly available as of the date of publication. Accession numbers are listed in the key resources table.
- All original code has been deposited at GitHub and is publicly available as of the date of publication. DOIs are listed in the key resources table.
- Any additional information required to reanalyze the data reported in this paper is available from the lead contact upon request.

EXPERIMENTAL MODEL AND SUBJECT DETAILS

Human blood samples

Acquisition of human blood samples and the experiments that were performed with them were approved by the Human Research Ethics Committee at the Walter and Eliza Hall Institute (WEHI HREC #18_09LR). Buffy coats were obtained from anonymous blood donors through the Australian Red Cross Blood Service (HREC #18-11VIC-06, #21-01VIC-02).

Mycobacterium tuberculosis single cell stock generation

T25 flasks (Sigma Aldrich) containing 10 mL 7H9 (Difco™ Middlebrook 7H9 broth, Becton Dickinson)/ADC (Becton Dickinson) media containing 0.05% Tween-80 (Sigma-Aldrich) were inoculated with 500 µL frozen aliquots of a lineage 2 clinical isolate of *Mtb* from South Africa. Flasks were incubated at 37°C for 10 days. Cultures were transferred to 50 mL Falcon tubes (Fisher Scientific) using a serological pipette on day 10

during exponential growth phase. One millilitre of culture was transferred to a 500 mL flask containing 100 mL 7H9/ADC media without Tween-80 and incubated at 37°C for a further 10 days, swirling intermittently after day four. On day 10, 50 mL aliquots were centrifuged at 3000 x *g* for 5 minutes at room temperature. Supernatants were removed and ~10 glass beads (2-3 mm, Sigma-Aldrich) were added to the pellets and shaken vigorously for 1 minute. Six mL Dulbecco's phosphate-buffered saline (DPBS, ThermoFisher) was added to each tube and mixed by inversion before allowing clumps to decant for 10 minutes. The upper 5 mL was decanted into a separate tube and centrifuged at 260 x *g* for 10 minutes at room temperature. The upper 4.5 mL of supernatant was transferred into a new tube containing 0.5 mL 50% glycerol (ThermoFisher) and aliquots stored at −80°C. One frozen aliquot was serially diluted in quadruplicate for plating on three-sector 7H10 (Difco™ Middlebrook 7H10 agar, Becton Dickinson)/ADC plates for colony forming unit (CFU) determination, incubated at 37°C and counted after 10, 14 and 21 days.

SARS-CoV-2 stock preparation

Vero (CCL-81, ATCC) cells were cultured in T-150 flasks in Dulbecco's Modified Eagle Medium (DMEM + 1 g/L D-glucose, L-glutamine and 110 mg/L sodium pyruvate, ThermoFisher) + 10% heat-inactivated foetal bovine serum (FBS, Sigma-Aldrich) until confluent. Media was removed and adherent cells were washed twice with DPBS before replacing with serum-free DMEM. A single 1 mL vial of VIC001 (24/03/21) SARS-CoV-2 stock (1×10^6 tissue culture infectious dose 50 [TCID50]/mL, obtained from The Peter Doherty Institute for Infection and Immunity, Melbourne, Australia) was thawed. Infection media was made up by adding VIC001 stock to serum-free DMEM to achieve an MOI of 0.01 (1×10^5 TCID50 for ~1×10^7 cells) and adding TPCK-treated trypsin (ThermoFisher) to a final concentration of 1 μg/mL. 2.5 mL of infection media was added to the Vero cells in the flask after removing the serum-free media and incubated at 37°C with 5% CO_2 for 30 minutes. Twenty millilitres of serum-free DMEM + TPCK trypsin was added to the flask and incubated at 37°C with 5% CO_2 for 48 hours or until sufficient cytopathic effect was observed under the microscope.

Vero cells were seeded in flat-bottomed 96-well plates (ThermoFisher) at a density of 1×10^4 cells/well and incubated at 37°C with 5% CO_2 overnight to achieve confluency. Media was removed from wells and cells were washed twice with DPBS before replacing with 125 μL of DMEM + TPCK trypsin. Infection media was removed from the T-125 flask, transferred to a 50 mL Falcon tube and centrifuged at 2000 x *g* for 5 mins to pellet the debris. Supernatant was transferred to a separate 50 mL Falcon tube, taking care to avoid the pellet, and then aliquoted into 1 mL Nunc® CryoTubes® to be stored at −80°C. One aliquot was used to measure TCID50 of the stock by diluting in 1:7 serial dilutions five times with six replicates in serum-free DMEM + TPCK trypsin in a round-bottom 96-well plate (ThermoFisher). Twenty-five microlitres of each dilution was transferred to the appropriate well of the 96-well Vero plate and incubated for four days at 37°C with 5% CO_2. TCID50 values were calculated by scoring wells (positive or negative) for cytopathic effect (CPE) on day four, using the Spearman and Kärber method (Ramakrishnan, 2016).

Monocyte culture

Peripheral blood mononuclear cells (PBMCs) were isolated from buffy coats by density gradient centrifugation with Lymphoprep (StemCell Technologies). Monocytes were isolated from PBMCs using CD14 MicroBeads (human, Mintenyi Biotec) and magnetic column separation (LS columns, QuadroMacs™ Separator, Miltenyi Biotec). Monocytes were differentiated into GM-CSF-polarised monocyte derived macrophages (MDMs) by incubation for seven days in RPMI 1640 media (ThermoFisher) + L-glutamine (1 mM, Gibco) + sodium pyruvate (2 mM, Gibco) + 10% human AB serum (Sigma-Aldrich), in the presence of 5 ng/mL GM-CSF (Miltenyi Biotec) at 37°C with 5% CO_2.

Macrophage culture

On day 7, MDMs were harvested using Accutase (Sigma-Aldrich) and seeded in flat-bottomed 96-well plates at a density of 1×10^5 MDMs per well in 200 μL RPMI 1640 media + L-glutamine + sodium pyruvate + 5% human AB serum.

METHOD DETAILS

Search strategy, selection criteria and data extraction

A literature search of published and pre-print COVID-19 manuscripts was conducted on the NIH PubMed and bioRxiv, medRxiv, and SSRN servers uploaded/published between 01/02/20 and 20/09/20 (Figure S1). We conducted our search of published manuscripts on NIH PubMed using the terms ((COVID-19[Title]))

AND (single-cell[Title/Abstract]) and pre-print manuscripts on the bioRxiv, medRxiv, and SSRN servers using the terms (ABSTRACT:"single-cell" OR ABSTRACT:"transcriptome sequencing" OR ABSTRACT:"whole-blood transcriptomic" OR ABSTRACT:"immunophenotyping") AND (TITLE:"COVID-19″) AND (FIRST_PDATE:[2020-02-01 TO 2020-09-20]) AND (SRC:PPR). We did not apply a lower date restriction but concluded our search on the 20/09/20. A total of 50 and 65 studies met the published and pre-print manuscript search criteria, respectively. These studies were further restricted to those conducted in humans, with sequencing performed on WB, PBMCs, or BALF, and from which DEGs could be obtained either directly from the text, figures, supplementary data or from publicly available sequence data. Studies which only included data from patients receiving experimental treatment were excluded. Nine COVID-19 datasets (Arunachalam et al., 2020; Hadjadj et al., 2020; Huang et al., 2020; Liao et al., 2020; Silvin et al., 2020; Wei et al., 2020; Wen et al., 2020; Wilk et al., 2020; Xiong et al., 2020) (Table 1, Figures S1 and S2) met the inclusion criteria and were used to generate tissue-, cell-, or pathway-level signatures of varied severity risk (Table S1). An additional WB influenza microarray dataset (Dunning et al., 2018) was downloaded from GEO (GSE111368) and was used to generate an influenza virus control signature by contrasting healthy controls with H1N1 patients, serving as a respiratory viral control set.

Inherent publication bias was mitigated as far as possible by selecting all available genes signatures, arising from all tissue and cell sources, identified in all published manuscripts, including preprints. Due to the rapid emergence of COVID-19, all results were deemed of scientific interest during the early phase, reducing the likelihood of positive correlation bias through lack of reporting of negative results. Publication bias of the identified COVID-19 and influenza signatures were quantitatively assessed by generating funnel plots that graph the area under the receiver operating characteristic curve (AUC) against the standard error of the AUC (Figure S3) (van Enst et al., 2014). AUC values were calculated by comparing the performance of each of the COVID-19/influenza signatures, assessed using the TBSingatureProfiler R package, for each of seven TB dataset groups compared to the London latent control group (*see* Table 2, TB contacts cohort). The Egger's test was performed as a quantitative measure of asymmetry in the funnel plot, using the The R package metafor (Viechtbauer, 2010). The AUC metric and corresponding standard error for each group on each signature were calculated using the R package pROC. Severe asymmetry either side of the overall effect line in the centre and an Egger's test p-value <0.05 indicates the possibility of publication bias (Figure S3). However, as many of these COVID-19 signatures were derived from specific cell populations they would be expected to show bias towards datasets that arise from disease states that are disproportionally enriched for those cells. As such the most common signatures with publication bias, representing disproportionate enrichment of the signatures across the tested TB datasets where MN, BALF and WB derived, which we identified to be enriched in active and progressive TB disease datasets (Figure 1).

The curatedTBData package (Wang, 2020), which includes 48 publicly available TB RNA-seq datasets, was used to identify and download eligible TB datasets, that included RNA-seq conducted on WB samples obtained from adolescents or adults, who had LTBI, active TB, and those with LTBI who progressed to TB during the duration of study follow-up, with RNA-seq data at baseline and time of diagnosis, and patient-level meta-data including time to TB progression. Of the ten datasets that were generated using Illumina RNA-seq from WB (excluded PBMC only, GSE112104), from HIV-negative (excluded HIV-positive, GSE107104) participants across the spectrum of latent, progressor, and active TB disease (excluded GSE89403 and GSE107105), five datasets from three studies (Singhania et al., 2018; Suliman et al., 2018; Zak et al., 2016) remained for signature profiling. These datasets and information on their constituent cohorts are listed in Table 2.

Profiling for COVID-19 risk

Eligible COVID-19 and influenza control signatures (Table S1) were evaluated independently against the patient-level TB RNA-seq data, generating individual-sample putative "COVID-19 risk score". To do this, the 36 COVID-19/influenza signatures were aggregated into an object of class *list* in RStudio (R version 4·0·2) (R Core Team, 2020). Each signature was used separately to generate the putative "COVID-19 risk score" by applying a gene set variation analysis (GSVA) (Hänzelmann et al., 2013) with the TBSignatureProfiler package (Jenkins et al., 2020). GSVA uses enrichment scoring which compares the rankings of the genes in a particular signature compared to all the other genes in that sample. Briefly, the composite gene list was mapped onto the gene expression statistics for each condition in the input TB dataset to generate a single enrichment summary statistic for each sample corresponding to an increased or decreased risk of COVID-19, depending on how the signatures were defined in the original

datasets. COVID-19 risk scores were correlated with TB outcomes and a two-sided t-test was used to determine the significance of these differences, with Bonferroni correction to adjust for multiple testing. A full list of significance values for each comparison can be found in (Tables S2, S3, S4, and S10).

Single-cell integrative analysis

Single cell RNA-seq integrative comparison was conducted using the identified COVID-19 BALF dataset (Liao et al., 2020) downloaded from the NIH GEO database (GSE145926) and a TB PBMC dataset (Cai et al., 2020) downloaded from NCBI Short Read Archive (SRA, SRR11038989-SRR11038995). Datasets were converted to fastq format using the *fastq-dump* function from the SRA toolkit and aligned to the GRCh38 human reference genome and sorted by barcode and the unique molecular identifier (UMI) using the CellRanger (version 4.0) *count* pipeline. *filtered_feature_bc_matrix.h5* files were read into RStudio using the Seurat *Read10X_h5* function (v3.0) (Stuart et al., 2019). Both datasets were independently normalised before the Seurat *FindIntegrationAnchors* function was applied to generate a corrected data matrix to facilitate a joint analysis. A principal component analysis (PCA) was applied to this matrix to scale the data for tSNE dimensionality reduction (Satija et al., 2015) using the first 20 principal components. Identified clusters were annotated using a combination of scCatch (Shao et al., 2020) to find marker genes associated with blood and lung tissues and the cluster markers identified in the original analysis of the BALF dataset (Liao et al., 2020). The following immune cell markers were derived from this manuscript: *CD68*, macrophages; *FCGR3B*, neutrophils; *CD1C* and *CLEC9A*, myeloid dendritic cells (mDCs); *LILRA4*, plasmacytoid dendritic cells (pDCs); *KLRD1*, NK cells, *CD3D*, T cells; *MS4A1*, B cells; *IGHG4*, plasma cells; *TPPP3* and *KRT18*, epithelial cells. Three genes - *FCN1*, *SPP1* and *FABP4* - were also used to identify the macrophage subpopulations discovered in the original analysis.

Functional enrichment analysis

The Leicester cohort of the TB combined cohort and the influenza H1N1 data (GSE107994 and GSE111368, respectively) were chosen to compile TB and influenza DGE lists for use in functional enrichment analyses on the basis that they consisted of the full spectrum of TB disease states and adequate control samples to generate disease-specific signatures. Differential gene expression (DGE) analysis was performed using *limma* (Ritchie et al., 2015) and a false-discovery rate-adjusted p-value (Haynes, 2013) threshold of <0·05 with an absolute $\log_2$ fold-change (LFC) >0·58 was used as a threshold for defining significant genes. A combined gene list from the WB COVID-19 study (Silvin et al., 2020) was derived from all populations identified by scRNA-seq and combined into an "all cell population DEGs" table by the authors and provided with corresponding $\log_2$ fold change (LFC) values as a supplementary table. To determine the enrichment of genes according to disease severity in COVID-19, bulk RNA-seq data from PBMCs grouped according to COVID-19 severity (Arunachalam et al., 2020) (GSE152418) were obtained and re-analysed for DEGs. To avoid superficial terms, the top 1000 DEGs (based on q-value cut-off 0·01) from the datasets were used and the enrichment calculated using the Metascape online pathway analysis portal (https://metascape.org/gp/index.html#/main/step1) (Zhou et al., 2019). Briefly, upon submission of a multiple gene list, the lists are merged to a common list, keeping the original membership disease/condition intact. To find statistically enriched ontology terms the following ontology sources were selected: KEGG, Gene Ontology Biological Processes, Reactome, Hallmark Gene Sets from MSigDB, Canonical Pathways, CORUM. For each ontology term a hypergeometric test with Benjamini-Hochberg correction (Haynes, 2013) was performed with a significant threshold corrected p-value <0·01. Accumulative hypergeometric corrected p-values and enrichment factors (>1·5) were calculated and used for filtering. Remaining significant terms were then hierarchically clustered into a tree based on Kappa-statistical similarities among their gene memberships (kappa 0·3 applied as a threshold). A full list of pathways and associated genes can be found in Table S11.

Protein-protein interaction and gene set enrichment analysis

Input gene lists from the functional enrichment analysis derived from the top 1000 DEGs across disease states were used to generate a PPI network from the following databases: BioGrid8 (Oughtred et al., 2019), InWeb_IM (Li et al., 2017), and OmniPath (Türei et al., 2016). Molecular Complex Detection (MCODE) algorithm (Bader and Hogue, 2003) was used to identify enriched clusters from the merged network. A GO enrichment analysis was applied to the original PPI network and its MCODE network components to assign biological "meanings", where the top three p-value terms were retained. The ten MCODE networks either with significant DEG or with annotations within the top 100 enriched pathways for COVID-19 were plotted as gene clusters as defined by MCODE. The shared gene cluster network

analysis was implemented in Gephi and visualized using Cytoscape (Shannon et al., 2003). Ranked GSEA was performed using GSEA (version 4·01) (Subramanian et al., 2005) . Genes from the cluster analysis were used as the gene set input (.gmt file) and LFC-ranked DEGs from the PBMC bulk RNA-seq dataset (Arunachalam et al., 2020) were profiled for enrichment.

Macrophage infection

MDMs were infected with *Mtb* at an MOI of 1 (1 × 10^5 CFU) for 4 hours at 37°C, or left uninfected as control. Media was removed from all wells after 4 hours and replaced with fresh RPMI complete media for a further 48 hours. *Mtb*-infected and uninfected MDMs were lysed with TRIzol reagent (Life Technologies) to extract RNA for gene expression analysis after 24, 36 and 48 hrs. Supernatants from 48 hr *Mtb* infections (conditioned media) were double filtered (96-well plate 0.2 PVDF filter membrane, Corning) to remove bacteria and added to uninfected MDMs at a 1:10 dilution. Conditioned media-treated MDMs were incubated for 48 hours at 37°C to induce a "bystander effect". These MDMs were then infected with SARS-CoV-2 at an MOI of 1 (1 × 10^5 viral particles) in the presence of TPCK trypsin (ThermoFisher) for 72 hours, after which MDMs were lysed with TRIzol reagent as above.

RT-PCR

RNA was separated from TRIzol samples using Phasemaker tubes (Life Technologies) with addition of chloroform:isoamyl alcohol (49:1 v/v, Sigma-Aldrich) and precipitated with isopropanol (Sigma-Aldrich), sodium acetate (Sigma-Aldrich) and linear polyacrylamide (Life Technologies) at −20°C overnight. Precipitated RNA was washed twice with 80% ethanol (Sigma-Aldrich) before final resuspension in distilled H_2O (dH_2O). 100-200 ng RNA from MDM was reverse transcribed using High Capacity cDNA synthesis kit (Applied Biosystems) and real-time RT-PCR was performed with Fast SYBR Green chemistry (Applied Biosystems), using 10% cDNA on Viia7 system (Applied Biosystems), with 60°C annealing temperature and 40 cycles. Melt curve analysis was performed to confirm amplicon specificity. Absolute quantification was carried out for *ACE1*, *ACE2*, *IL1B*, *IL6*, *IFNA1*, *IFNB1*, *IFNG*, *TMPRSS2*, *TNF* using synthesised primers (Integrated DNA Technologies, IDT) and standard curves generated by serial dilution of target amplicon-containing plasmids (pGEM-T easy, Promega), to cover up to 6 logs of amplicon copy number per microliter and absolute copy number normalized to *RPL13A*.

SARS-CoV-2 RNA was quantified using a primer-probe qPCR assay for SARS-CoV-2 Nucleocapsid-1 (N1) (IDT) and an iTaq Universal Probes One-Step Kit (Bio-Rad), according to manufacturers' instructions. Samples were run on the Viia7 system using FAM dye set as the reporter and ROX as the passive reference. *N1* mRNA Ct values were normalised to housekeeping gene *RPL13A* and fold change to no conditional media controls calculated using $2^{-\Delta\Delta Ct}$.

QUANTIFICATION AND STATISTICAL ANALYSIS

R software was used to perform data and statistical analyses. Statistical details are provided in the respective figure legends and Method details sections. The Egger's test was performed as a quantitative measure of asymmetry of funnel plots. Two-sided t-test was used to determine the significance of differences between COVID-19 risk scores, with Bonferroni correction to adjust for multiple testing. TCID50 values were calculated using the Spearman and Kärber method (Ramakrishnan, 2016). PCR Ct values were normalised to the relevant control values using $2^{-\Delta\Delta Ct}$. A false-discovery rate-adjusted p-value (Haynes, 2013) threshold of <0·05 with an absolute LFC >0·58 was used as a threshold for defining significant genes in DGE analyses. Hypergeometric tests with Benjamini-Hochberg correction (Haynes, 2013) were performed with a significant threshold corrected p-value <0·01 to determine gene ontology enrichment; accumulative hypergeometric corrected p-values and enrichment factors (>1·5) were calculated and used for filtering.